

**Age and Anatomy of the Gongga Shan batholith, Eastern Tibetan Plateau and its relationship to the active Xianshui-he fault.**

M.P. Searle<sup>1</sup>, N.M.W. Roberts<sup>2</sup>, S-L. Chung<sup>3,4</sup>, Y-H. Lee<sup>5</sup>, K.L. Cook<sup>3,6</sup>, J.R. Elliott<sup>1</sup>, O.M. Weller<sup>7</sup>, M.R. St-Onge<sup>7</sup>, X. Xu<sup>8</sup>, X. Tan<sup>8</sup>, and K. Li<sup>8</sup>.

1. *Department of Earth Sciences, Oxford University, South Parks Road, Oxford OX1 3AN, UK.*
2. *NERC Isotope Geosciences Laboratory, British Geological Survey, Keyworth, Nottingham, UK.*
3. *Department of Geosciences, National Taiwan University (NTU), Taipei 10617, Taiwan.*
4. *Institute of Earth Sciences, Academia Sinica, Taipei 11529, Taiwan.*
5. *Department of Earth and Environmental Sciences, National Chung-Cheng University, Chiayi, Taiwan.*
6. *Now at: GFZ German Research Center for Geosciences, Telegrafenberg, 14473 Potsdam, Germany.*
7. *Geological Survey of Canada, 601 Booth Street, Ottawa, Ontario K1A 0E8, Canada.*
8. *Institute of Geology, China Earthquake Administration, Huayanli A1, Chaoyang district, Beijing 100029, China.*

## **Abstract**

The Gongga Shan batholith of eastern Tibet, previously documented as a ~32 – 12.8 Ma granite pluton, shows some of the youngest U-Pb granite crystallisation ages recorded from the Tibetan plateau, with major implications for the tectonothermal history of the region. Field observations indicate that the batholith is composite, with some localities showing at least seven cross-cutting phases of granitoids that range in composition from diorite to leucocratic monzogranite. In this study we present U-Pb ages of zircon and allanite dated by LA-ICPMS on seven samples, to further investigate the chronology of the batholith. The age data constrain two striking tectonic-plutonic events: a complex Triassic-Jurassic (ca. 215-159 Ma) record of biotite-hornblende granodiorite, K-feldspar megacrystic granite and leucogranitic plutonism, and a Miocene (ca. 14-5 Ma) record of monzonite-leucogranite emplacement. The former age range is attributed to widespread 'Indosinian' tectonism, related to Paleo-Tethyan subduction zone magmatism along the western Yangtze block of South China. The younger component may be related to localised partial melting (muscovite-dehydration) of thickened Triassic flysch-type sediments in the Songpan-Ganze terrane, and are amongst the youngest crustal melt granites exposed on the Tibetan Plateau. Zircon and allanite ages reflect multiple crustal re-melting events, with the youngest at ca. 5 Ma resulting in dissolution and crystallization of zircons and growth/resetting of allanites. The young garnet, muscovite and biotite leucogranites occur mainly in the central part of the batholith and adjacent to the eastern margin of the batholith at Kangding where they are cut by the left-lateral Xianshui-he fault. The Xianshui-he fault is the most seismically active strike-slip fault in Tibet and thought to record the eastward extrusion of the central part of the Tibetan Plateau. The fault obliquely cuts all granites of the Gongga Shan massif and has a major transpressional component in the Kangding – Moxi region. The course of the Xianshui Jiang river is offset by ~62 km along the Xianshui-he fault and in the Kangding area granites as young as ~5 Ma are cut by the fault. Our new geochronological data show that only a part of the Gongga Shan granite batholith is composed of young (Miocene) melt, and we surmise that as most of eastern Tibet is composed of Precambrian – Triassic Indosinian rocks there is no geological evidence to support regional Cenozoic internal thickening or metamorphism and no evidence for eastward directed lower crustal flow away from Tibet. Instead we suggest that

underthrusting of Indian lower crust north as far as the Xianshui-he fault resulted in Cenozoic uplift of the eastern plateau.

## INTRODUCTION

The Tibetan Plateau (Fig. 1) is the world's largest area of high elevation (~5 km average) and thick crust (70-85 km thick), and the timing of its rise is important not only for tectonics but also for understanding the influence of topography on climate and the erosional flux of sedimentary detritus into rivers and oceans. Geological evidence for crustal thickening and topographic uplift includes the timing of compressional deformation, regional metamorphism and magmatism. Earlier notions of a Late Cenozoic thickening and rise of the Tibetan plateau (e.g. Molnar et al., 1993) following the Early Eocene collision of India with Asia and the closing of the intervening Neo-Tethys ocean at 50.5 Ma (Green et al., 2008) have since been challenged by more recent geological investigations. Chung et al. (2005), Kapp et al. (2007) and Searle et al. (2011) noted the widespread occurrence of Andean-type subduction-related Late Jurassic – Early Eocene granites (Ladakh-Gangdese batholith) and calc-alkaline volcanic rocks across the Lhasa block strongly suggesting an Andean-type topography with similar crustal thickness during the period prior to the India-Asia collision. Soon after India-Asia collision, calc-alkaline Gangdese-type magmatism ended (St-Onge et al., 2010) and volumetrically minor, sporadic but widespread adakitic magmatism occurred across the plateau since 50 Ma (Chung et al., 2005).

The present-day structure of eastern Tibet is characterised by a high, flat plateau, with a few exceptional topographic anomalies, such as the Gongga Shan (7556 m) massif, and a steep eastern margin along the Longmen Shan, showing an abrupt shallowing of the Moho from depths of 60-80 km beneath the plateau to depths of 35-40 km beneath the Sichuan basin (Zhang et al., 2010). There is an almost complete lack of Cenozoic shortening structures, with the exception of steep west-dipping faults associated with the M7.9 Wenchuan earthquake along the Longmen Shan margin (Hubbard and Shaw, 2009). Most of the deformation in eastern Tibet is Indosinian (Triassic-Jurassic) in age (Harrowfield and Wilson, 2005; Wilson et al., 2006; Roger et al., 2008). The thick Triassic Songpan-Ganze 'flysch' sedimentary

rocks are tightly folded about upright fold axes and lie above a major horizontal detachment above Palaeozoic basement (Harrowfield and Wilson, 2005). Most granites that have been dated intruded during the period 220-188 Ma (Roger et al., 2004, 2008; Zhang et al., 2006). A complete Barrovian-type metamorphic sequence is present in the structurally deeper Danba dome, where peak sillimanite grade metamorphism has been dated at  $179.4 \pm 1.6$  Ma using *in situ* U-Pb monazite analysis (Weller et al., 2013). There is no record of any Cenozoic metamorphism anywhere in north, east or central Tibet. The old ages of deformation, metamorphism and magmatism argue strongly against the Miocene-recent homogeneous crustal shortening models for Tibet (Dewey and Burke, 1973; England and Molnar, 1979).

Cenozoic structures in central and eastern Tibet are represented by large-scale strike-slip faults (Fig. 2). The Ganzi (Yushu) and Xianshui-he left-lateral strike-slip faults cut across all the geology of the eastern plateau and have diverted river courses in the upper Yangtze and Jinsha river systems. These faults curve around the Eastern Himalayan syntaxis and are thought to be responsible for southeastward extrusion of the south Tibetan crust (Molnar and Tapponnier, 1975; Peltzer and Tapponnier, 1988; Peltzer et al., 1989; Tapponnier et al., 2001) and clockwise rotations caused by the northward indentation of India (England and Molnar, 1990).

Along the Xianshui-he fault a granitic batholith, the Gongga Shan massif, crops out for about 200 km along the southwestern margin (Fig. 3). This forms a major topographic high, with the Gongga Shan massif reaching 7756 meters. Roger et al. (1995) reported a granite emplacement U-Pb zircon age of  $12.8 \pm 1.4$  Ma for one sample from the western margin of the batholith along the Kangding – Yadjang road. They also reported Rb/Sr cooling ages from a deformed granite of  $11.6 \pm 0.4$  Ma and an undeformed granite of  $12.8 \pm 1.4$  Ma and  $9.9 \pm 1.6$  Ma. Liu et al. (2006) sampled the same granite and obtained a SHRIMP U-Pb age of  $18.0 \pm 0.3$  Ma. Li and Zhang (2013) reported SHRIMP U-Pb zircon ages of  $\sim 31.8$  Ma and  $\sim 26.9$  Ma for a leucosome and melanosome collected from the eastern margin near Kangding and ages of 17.4 Ma and 14.4 Ma from the main granite pluton. These authors interpret the ages as resulting from a stage of metamorphism and migmatization at 32 to 27 Ma and magma intrusion at 18 to 12 Ma. The Gongga Shan granites are some of the rare examples of Cenozoic crustal melts exposed on the Tibetan plateau and therefore a study of their ages and origin is important in connection with the proposed crustal

models particularly the wholesale underthrusting model of Argand (1924) and the lower crust flow model of Royden et al. (1997) and Clark and Royden (2000).

We studied three main transects across the Gongga Shan batholith along the Kangding, Yanzigou and Hailugou valleys (Fig. 4) and collected samples for petrology and U-Pb geochronology. In this paper we first summarise the geology of eastern Tibet and discuss geophysical constraints on the structure of the deep crust, notably evidence for the timing of crustal thickening and Cenozoic crustal melting. We describe the Xianshui-he fault and present new field observations for the Gongga Shan batholith, that provide constraints on the emplacement history of different plutonic phases, for which we provide new *in situ* U-Pb zircon and allanite age data. We then use the timing constraints on the granite batholith to infer the age of initiation, and offset along the Xianshui-he fault. Finally, we use our new data on the Gongga Shan granites and the Xianshui-he fault to discuss the models for the tectonic evolution of the Tibetan plateau.

## **GEOLOGY AND TECTONIC SETTING OF EAST TIBET**

Widespread Neoproterozoic granitoids and gneisses record the cratonisation of the Yangtse block across South China. The Kangding complex outcropping along the eastern margin of the Xianshui-he fault has SHRIMP U-Pb zircon ages of  $797 \pm 10$  Ma to  $795 \pm 13$  Ma, roughly contemporaneous with several other gneiss complexes along the western margin of the Yangtse block (Zhou et al., 2002). Rifting led to the opening of the Palaeo-Tethys Ocean across north Asia and the initiation of several subduction zone systems along the KunLun – Anyemaqen terrane to the north (220-200 Ma granite batholiths), Jinsha suture to the south and the Yushu-Batang zone to the east (Roger et al., 2004, 2010). During the middle Permian the rifting of Neo-Tethys to the south isolated the Qiangtang block which became one of the Cimmerian micro-continental plates within Tethys (Sengor, 1985). The huge Emeishan continental flood basalt eruptions at ~260 Ma (Xu et al., 2001; Song et al., 2004) led to extensional rifting and formation of the Songpan-Ganze basin. The Songpan-Ganze terrane shows a thick sequence of Triassic sedimentary rocks in this branch of the Palaeo-Tethys. Convergence between the Qiangtang terrane and the North and South China blocks led to closure of the Songpan-Ganze Ocean and the major Late Triassic-

early Jurassic Indosinian orogeny. This is evidenced by large-scale regional upper crustal shortening across the Songpan-Ganze terrane (Harrowfield and Wilson, 2005) and lower crustal regional metamorphism recorded from the Danba structural culmination (Weller et al., 2013). Eastern Tibet has been elevated above sea-level since the Late Triassic-Jurassic and there is no evidence of any later tectonic events until the Late Cenozoic.

In eastern Tibet crustal thickness beneath the Songpan-Ganze and KunLun terranes is approximately 70 km, shallowing to about 54 km beneath the Tsaidam (Qaidam) basin to the north (Mechie and Kind, 2013). Moho depths decrease from ~60 km beneath the eastern part of the plateau to 40-36 km beneath the Sichuan basin (Zhang et al., 2010). This corresponds to a very steep topographic boundary along the Long Men Shan mountains, the eastern border of the plateau. The Qiangtang terrane crust south and west of the Xianshui-he fault is a zone of anomalous low velocities ( $<3.3 \text{ km/sec}^{-1}$ ), strong radial anisotropy (Huang et al., 2010), high Poisson's ratios (Xu et al., 2007) and high electrical conductivity in the middle crust (Bai et al., 2010). These data imply that the lower 10-15 km of crust in eastern Tibet is strong and has no 'flow' characteristics, whereas the middle crust is weak and may have interconnected fluids promoting some form of flow (Liu et al., 2014). The Songpan-Ganze terrane, north of the Xianshui-he fault is a zone of higher crustal viscosity with less, or no, fluids in the middle crust. This area is characterised by regional Triassic-Jurassic Indosinian metamorphism (Weller et al., 2013) and has no evidence of Cenozoic crustal shortening, folding or metamorphism.

The eastern margin of the Tibetan Plateau is marked by the LongMen Shan range which shows steep west-dipping thrust faults, like that which ruptured during the 2008 Wenchuan earthquake (Hubbard and Shaw, 2009), exhuming old, Precambrian and Palaeozoic rocks along the hanging-wall (Baoxing, Pengguan massifs). The eastern margin of Tibet is completely different from the southern, Himalayan margin. In the LongMen Shan there is no regional Cenozoic metamorphism or crustal melting as seen along the Himalaya, there is no Main Central Thrust equivalent structure, no South Tibetan Detachment type structure and thus no evidence for any kind of channel flow (Searle et al., 2011). A model of eastward directed flow of the lower crust from beneath the Tibetan plateau was proposed by Royden et al. (1997) and Clark and Royden (2000) to explain the tectonic features of eastern Tibet and Yunnan. GPS data records the eastward-directed

motion of the upper crust of East Tibet with motion appearing to ‘flow’ around the stable Sichuan basin (Gan et al., 2007). These GPS data however record present day motion of the surface, nothing about deep crust motion. However, recent seismic data supports a strong lowermost crust under all of Tibet (Lhasa and Qiangtang terranes) and a weak middle crust (Tilmann et al., 2003; Mechie and Kind, 2013). Unlike the partially molten middle crust of southern Tibet, which is laterally connected with the Cenozoic metamorphism along the Himalaya, there is no such boundary along the eastern margin of Tibet in the LongMen Shan. The lower crustal flow models for Eastern Tibet proposed by Royden et al. (1997) and Clark and Royden (2000) are not grounded in geological observations or data. If the lower crust did flow around the stable Sichuan block this is not reflected in the mapped surface bedrock geology and there is no evidence to support contemporary upper crustal shortening in East Tibet, nor documentation in the geology of Sichuan or Yunnan for Tibetan rocks flowing to the east and southeast.

There is some geological evidence for small-scale post-50 Ma localised partial melting of the Tibetan lower crust (forming adakites; Chung et al., 2003, 2005; Wang et al., 2010) and middle crust (forming leucogranites, rhyolites; Wang et al., 2012) as well as some young (up to ca. 8 Ma) leucogranitic magmatism along the NyenchenTanggla (Liu et al., 2004; Kapp et al., 2005; Weller et al., 2016). Although there is some geophysical (seismic and magnetotelluric data) evidence for present-day low-degree partial melting, there is no evidence for widespread mid-crust sillimanite-grade migmatites and leucogranites such as seen along the Greater Himalaya (mid-crustal channel flow).

## **TIMING OF CRUSTAL THICKENING OF THE TIBETAN PLATEAU**

Strong evidence for Indosinian (Late Triassic-Jurassic) crustal thickening in Eastern Tibet comes from the regional folding and thrusting in Songpan Ganze sedimentary units. Late Triassic sedimentary rocks between 5-15 km thick show tight-upright folds and penetrative cleavage above a major regional detachment separating low-grade or unmetamorphosed sedimentary rocks above from Proterozoic basement rocks beneath (Harrowfield and Wilson, 2005). A lack of post-Triassic sedimentary rocks on the East Tibetan plateau suggest that it may have been topographically above

sea-level since then. Late Triassic crustal thickening led to regional Barrovian metamorphism, which is exposed in the exhumed Danba antiform where amphibolite facies kyanite and sillimanite-grade metamorphism has been dated by U-Pb monazite at 192-180 Ma (Weller et al., 2013).

There is evidence for regional metamorphism in southern Tibet at ca 200 Ma (Weller et al., 2015a) followed by regional magmatic crustal thickening along southern Tibet (Gangdese ranges) during the late Jurassic to early Eocene (ca. 188 – 45 Ma; Chu et al., 2006; Wen et al., 2008; Chiu et al., 2009; Chung et al., 2009). Intrusion of the Gangdese I-type subduction-related calc-alkaline batholith and eruption of andesites, dacites and rhyolites occurred along the 2000 km length of the Trans-Himalayan batholith (Kohistan, Ladakh and Gangdese granites and extrusives). The geology of these ranges suggests a topographic uplift during the Jurassic to early Eocene, similar to the modern-day Peru-Bolivian Andes. An intense magmatic ‘flare-up’ around 50 Ma occurred along the Gangdese batholith as volcanic compositions ranged from calc-alkaline to shoshonitic and adakitic (Lee et al., 2009). Shoshonitic volcanics imply a deep, hot mantle and lower crust-derived adakites imply a thick continental crust. Abundant adakitic melts requiring a garnet-bearing amphibolite or eclogite lower crust source across Tibet occurred from 47 Ma in the Qiangtang terrane and since at least 30 Ma in the Lhasa terrane (Chung et al., 2005) implying that the whole of Tibet was crustally thickening and topographically high since the Early-Middle Eocene (Searle et al., 2011). Lower crustal felsic and mafic granulite xenoliths entrained in Cenozoic ultra-potassic shoshonites from the Lhasa and Qiangtang terranes also conclusively show that extreme crustal thickness must have been present across Tibet during the Miocene (Hacker et al., 2000; Chan et al., 2009).

Evidence for widespread plateau formation during the Late Cretaceous-Palaeogene (pre-45 Ma) also comes from regional  $^{40}\text{Ar}/^{39}\text{Ar}$ , Fission Track and [U-Th]/He data (Kirby et al., 2002; Hetzel et al., 2011; Rohrmann et al., 2012) which shows that large regions of the plateau underwent cooling and exhumation prior to 45 Ma coeval with up to 50% upper crustal shortening (Kapp et al., 2005, 2007). The Eocene low-relief plateau surface shows that the plateau was high and dry with very little erosion, similar to the present-day situation, since 45 Ma (Hetzel et al., 2011). Significant high topography existed across the entire Tibetan plateau before the India-Asia collision with pulses of rapid exhumation at 30-25 Ma and also at 15-10 Ma recorded by low-temperature thermochronology (Wang et al., 2012).

There is no geological or geochronological evidence to suggest that the Tibetan Plateau was uplifted only in the last 7-8 Ma as suggested by various lines of circumstantial evidence (e.g. Molnar et al., 1993). It may have enjoyed an increase in elevation during Late Cenozoic times but all lines of evidence point to the fact that the entire plateau was elevated above sea-level since mid-Cretaceous time, attained at least Andean (Bolivian Altiplano) type elevations during the Cretaceous-Eocene and was as thick as present day (ca 75-65 km) during the Miocene, probably since the Early Eocene.

## **XIANSHUI-HE FAULT**

The combined Ganzi-Yushu and Xianshui-he faults extends for about 1200 km length from the central part of the Tibetan plateau curving around towards the southeast and ending in a series of splays in western Yunnan, north of the Red River fault (Burchfiel et al., 1998; Wilson et al., 2006; Wang et al., 2014). The Xianshui-he fault is one of the most seismically active strike-slip faults of the Tibetan Plateau region with nine major earthquakes of M7 – M7.9 magnitude between 1725-1983 (Wang et al., 1998). Focal depths of earthquakes are down to 20 km depth suggesting active sinistral slip in the upper crust. Active slip rates were estimated at  $15 \pm 5$  mm/yr from dating fault offset material (Allen et al., 1991) and geodetic estimates of the current slip rate are estimated at 9-12 mm/yr from InSAR (Wang et al., 2009). Measured GPS slip rates suggest present day slip may be ~10-12 mm/yr (Zhang et al., 2004).

The main Xianshui-he fault runs along the eastern margin of the Gongga Shan massif but a series of en echelon sinistral faults cut across the batholith forming a classic left-lateral strike-slip duplex system (Fig. 4). From Chinese maps these fault strands each show only minor offsets of the granite margin between 5-10 km. One major fault strand cutting through Triassic meta-sediments to the west of Gongga Shan shows a spectacular gouge zone that can be traced for over 200 km from Barmie to Ganzi (Wilson et al., 2006). North of Kangding the Xianshui-he fault shows ductile fabrics as well as later brittle gouge zones. The ductile shearing fabrics die out to the west away from the fault indicating that both ductile and brittle movement along the fault post-dated granite emplacement. Around Kangding the fault shows a

transpressional uplifted western margin (Gongga Shan granite) with a >2 km topographic difference from the batholith west of the fault to the Kangding NeoProterozoic complex east of the fault. South of Kangding the Xianshui-he fault cuts through meta-sediments and Proterozoic gneisses east of the batholith. Two major NW-SE aligned fault splays cut the granite batholith and field relationships clearly indicate faulting came after granite emplacement (Fig. 4). Towards Moxi township the fault cuts through Palaeozoic meta-sedimentary rocks approximately 12 km to the east of the eastern intrusive margin of the Gongga Shan granite batholith. The trace of the Xianshui-he fault then heads south towards Kunming where again it splays into several different strands aligned at right-angle to the NW-SE aligned Ailao Shan – Red River shear zone (Burchfiel and Chen, 2012).

Total left-lateral displacement has been suggested as ~50-60 km based on dubious pinning points (e.g. Precambrian-Proterozoic unconformity on Chinese maps, and older faults that may not originally have been the same structure). From Chinese maps, offsets of the Gongga Shan granites may be only ~15 km along the western margin of the batholith and up to 60 km along the eastern margin. We now report our new findings from the Gongga Shan batholith of eastern Tibet.

## **GONGGA SHAN BATHOLITH FIELD RELATIONSHIPS**

The Gongga Shan batholith stretches for over 100 km in an arcuate trend across central east Tibet and is approximately 10-15 km wide (Fig. 4). The batholith is cut by strands of the left-lateral Garze – Yushu and Xianshui-he strike-slip faults, which stretch for more than 800 km from the central Tibetan plateau east and southeast into Yunnan. The faults cut across regional geology and clearly offset the Gongga Shan granites, although precise amount of offset is difficult to accurately constrain (Roger et al., 1995). We studied three major valleys transecting the Gongga Shan batholith: the main Kangding road, the Yanzigou valley, which cuts westward into the batholith just to north of Gongga Shan (7556 m), and the Hailuogou valley which runs west of Moxi town to the high peaks south of Gongga Shan.

### **Kangding road section**

The main road from Barmie to Kangding cuts across the central part of the Gongga Shan batholith. The western part of the batholith contains two main phases of granite, an earlier granodiorite and a later biotite granite. Sample BO-59 (Fig. 5a) was collected from a location close to the sample collected by Roger et al. (1995) which they dated at  $12.8 \pm 1.4$  Ma. The middle part of the batholith comprises a lithology: Kfs + Qtz + Pl + Bt monzogranite that forms most of the batholith (sample BO-62; Fig. 5b). Later minor intrusions of biotite + tourmaline pegmatites and secondary muscovite  $\pm$  garnet granite veins intrude the main phase. At the Shuguang bridge locality in the middle of the Kangding road section one outcrop show three distinct cross-cutting relationships (Fig. 5c). An earlier biotite monzogranite (BO-57) has a weak foliation and has been intruded by a second phase more leucocratic biotite  $\pm$  muscovite granite (BO-52) with migmatitic textures (schlieren of older melanosomes). Both lithologies are cut by a later undeformed pegmatite (BO-55). In places a younger phase of garnet leucogranite has intruded all previous lithologies (Fig. 5d) and along the northeastern margin of the batholith north of Kangding complex intrusive relations have been mapped (Fig. 5e). The youngest phase of intrusion in this transect is a fine-grained undeformed biotite microgranite (Fig. 5f) that cuts all previous lithologies.

The western margin of the Gongga Shan batholith appears to be a vertical intrusive contact (Fig. 6a). The granite along the western margin above the new Kangding airport south to the Zheduo Shan pass shows little or no fabric and there does not appear to be a contact aureole in the country rock (Triassic shales). The granite along the eastern margin has a vertical contact, cutting both fabrics in the country rocks to the east (Kangding complex) and internal fabrics within the granite. At Kangding four phases of granite intrusions have been mapped from early biotite monzogranite through to late garnet + biotite leucogranite cut by pegmatite dykes (Fig. 6b). Ductile foliations within the granites strike around  $028^\circ$  NNE oblique to and truncated by the strike of the Xianshui-he fault. South of Kangding and across the Baihaizi pass the Conch gully area shows a mixture of biotite + hornblende granodiorites with igneous enclaves (Fig. 6c), magmatic mixtures of more enclave-rich granite intermingled with the granodiorite (Fig. 6d) and more evolved garnet leucogranite (Fig. 6e, f).

### **Yanzigou valley (north Gongga Shan)**

The Yanzigou valley cuts west directly into the heart of the granite batholith immediately to the north of Gongga Shan. East-verging recumbent folds in probable Triassic meta-sediments (Fig. 7a) are truncated abruptly at the margin of the batholith (Fig. 7b). The oldest intrusions in the area are a series of foliated biotite + hornblende granodiorites (BO-76). Towards the west in the Swallow cliffs area and around the snout of the north Gongga Shan glacier leucogranites (BO-68) appear to be increasingly common with evidence of partial melting in meta-sedimentary migmatites. The leucogranites are always the younger intrusive phase, intruding into and breaking up enclaves of the more mafic granites (Fig. 7c,d). Multiple phases of granitoids are seen with clear cross-cutting relationships in spectacular outcrops in the middle part of the batholith (Figs. 7e,f, 8). The eastern margin of the batholith shows a prominent fabric striking  $160^{\circ}$  NW-SE and dipping at  $50^{\circ}$  NE. The fabric in the gneisses is abruptly truncated by the granite margin. The Xianshui-he fault in this profile is 11-12 km to the east of the granite contact and cuts through gneisses of the Kangding complex. Clearly the field relationships show that the granite batholith was not related to the strike-slip fault in any way.

#### **Hailuogou valley (Moxi, south Gongga Shan)**

The Hailuogou valley extends west of Moxi town into the highest peaks around Gongga Shan (7556 meters) itself (Fig. 9a). Glaciers have carved a deep gorge into the high country around the western part of the batholith but Gongga Shan itself is snow-covered and somewhat inaccessible. The granite contact along the eastern margin is vertical and clearly exposed along the northern rim of the Hailuogou valley (Fig. 9b). Foliations in the gneisses are near vertical at the contact but folded further to the east. Above the cable car station on the Gongga Shan glacier the dominant lithology is a hornblende + biotite diorite with K-feldspar megacrystic granite also containing hornblende and biotite (Fig. 9c). Igneous diorite enclaves are common in the granite (Fig. 9d). Boulders in the glacier and streams above the cable car station suggest that the Gongga Shan peak is composed of granodiorite. There is no sedimentary or country rock talus implying that the western margin of the batholith is west of the Gongga Shan summit. There is little evidence along the Hailuogou valley profile of the more garnet-bearing leucogranite or migmatite phases seen commonly in the Yanzigou valley to the north.

## U-PB GEOCHRONOLOGY

### Methods

Zircon, allanite and titanite were separated from seven granitic samples by standard techniques (crushing, milling, Rogers table, Frantz magnetic separation and heavy liquids). Grains were picked under alcohol and mounted in one-inch epoxy mounts. In order to guide analytical spot placement, zircon grains were imaged using cathodoluminescence (CL). Back scattered electron (BSE) imaging was conducted for allanite and titanite grains, but revealed no systematic zoning.

U-Pb geochronology utilised a Nu Instruments Attom single-collector inductively coupled plasma mass-spectrometer (SC-ICP-MS) coupled to a New Wave Research 193FX Excimer laser ablation system with an in-house teardrop shaped cell (Horstwood et al., 2003). The full method is described in Spencer et al. (2014). In brief, ablation used static spots ranging from 20-40  $\mu$  m depending on the size of the growth-zoning that the sample allowed. Ablation parameters were 5Hz at  $\sim 2\text{J}/\text{cm}^2$  for 30 seconds, with 10 second wash-out. Standard sample bracketing utilised the average drift-corrected ratios for 91500 (Wiedenbeck et al., 1995), or GJ-1 (Jackson et al., 2004) and Plešovice (Sláma et al., 2008) for normalisation of zircon; 40010 (Smye et al., 2014) for allanite, and Ontario-2 for titanite (Spencer et al., 2013). Data were reduced using an in-house spreadsheet, and Isoplot (Ludwig, 2003) was used for age calculation. Allanite age data were corrected for excess  $^{206}\text{Pb}$  due to initial  $^{230}\text{Th}$  disequilibrium, based on a whole-rock Th/U ratio of 3. This ratio is arbitrary and not sample-based, therefore, young ( $<50$  Ma) ages may be biased towards older by several percent (Smye et al., 2014). Intercept ages for allanite (except the free regression of BO76) use an upper intercept based on an assumed common-lead component as per Stacey & Kramers (1975) of  $0.83 \pm 0.2$ .

All analyses are plotted and ages are quoted at  $2\sigma$ . Imprecise ages based on intercepts, due to lead-loss or mixing, or those with excess scatter based on MSWD values (and presumably due to geological variation such as inheritance and lead-loss), are quoted as ca. xx Ma. Precise ages given with uncertainties, interpreted as individual crystallisation events, are quoted as age  $\pm \alpha / \beta$  Ma, where  $\alpha$  refers to the measurement and session-based uncertainty, and  $\beta$  is the total uncertainty after

propagation of systematic uncertainties (decay constants, reference material age uncertainty, long-term reproducibility of the laboratory method) (see Horstwood et al., accepted).

### **BO-52 Migmatitic biotite-muscovite granite, Shuguang bridge**

This sample gave a moderate zircon yield. Grains were a mixture of sizes, mostly elongate, from 100 to 200  $\mu\text{m}$  typically. The majority of grains show oscillatory zoning in CL, often with two apparent phases of growth; some with brighter cores and darker rims, and some with dark and recrystallized cores. Some grains have a thin rim, and some are fractured.

Forty analyses yield a spread of ages from 112 Ma to 179 Ma, and two core analyses gave older ages of ca. 235 Ma (Fig. 10). Two of the younger analyses gave ages ca. 35 Ma, and a third is slightly older at 51 Ma; these are from a CL dark overgrowth and recrystallised zones. There is no obvious single population from within the older ages, although the average of these falls at ca. 167 Ma (using TuffZirc; Ludwig, 2003). Overgrowths and thick rims on zircon are not exclusively related to younger ages, they extend up to 167 Ma. Only a few allanite analyses were obtained, and these exhibit some scatter. A tight cluster of analyses gives a regression with an age of ca. 173 Ma; this is within uncertainty of the oldest of the zircon age populations. A second array through analyses with a high radiogenic component gives an age of ca. 16 Ma, suggesting a younger allanite crystallisation/resetting event. The interpretation of the geochronological data is equivocal; however, we interpret the zircon and allanite data collectively as recording migmatization at ca. 16 Ma.

### **BO-55 Pegmatite, Shuguang bridge**

This sample gave a low zircon yield. The grains are typically 100 to 200  $\mu\text{m}$  long, and some are smaller. In CL, oscillatory zoning is exhibited, and this has been disturbed in some grains. Some grains are fractured, and some show evidence of recrystallisation. Thin rim overgrowths are not obvious, but a few grains show thicker zoned overgrowths that cut across internal zones.

The four oldest analyses overlap at  $159 \pm 2/4$  Ma (MSWD = 0.34) (Fig. 11). A younger population of analyses overlaps at ca. 41 Ma. Three more analyses overlap at 37 Ma, and may represent another distinct age population. Twelve further analyses spread from 22 Ma to 15 Ma, and may represent a single discordia that is recording

lead-loss from a ca. 41-37 Ma event, or from a ca. 159 Ma event. The youngest date recorded by a lead-loss trend is ca. 15 Ma. All of the younger populations were obtained on a mixture of recrystallized zones and zoned overgrowths, and there is no discernable change in Th/U ratio with age. Multiple overlapping ages from recrystallised zones at ca. 40 Ma imply this age is reflecting an actual crystallization event, and not solely due to lead-loss as this would generally be variable within a single grain.

Allanite exhibits an array with high common lead content, and probable mixing between two events. The oldest analyses define an array with a lower intercept at ca. 164 Ma; this is correlative to the oldest zircon ages. The youngest allanite grain records a lower intercept at ca. 15 Ma, which can be interpreted as a maximum age for the younger allanite growth/resetting event. The age of pegmatite crystallisation is interpreted to be ca. 15 Ma, with both older zircon and allanite ages reflecting inheritance from the protolith.

#### **BO-57 Deformed biotite monzogranite, Shuguang bridge**

This sample gave a moderate zircon yield. All grains are elongate igneous zoned zircons 100 to 250  $\mu\text{m}$  long, with planar or oscillatory zoning. There appears to be one main growth zone, although a few grains have brighter cores, and these are recrystallized in a few grains. Some outer rim regions exhibit resorption textures also. Thirty-two analyses define a population with an age of ca.  $182 \pm 1/4$  Ma (MSWD = 1.4) (Fig. 12). Two analyses are slightly older at 195 and 207 Ma, possibly reflecting inheritance, and one analysis is slightly younger at 166 Ma, probably representing lead-loss. Three distinctly older grains give Proterozoic ages (795 Ma, 969 Ma, 2469 Ma). The crystallisation age of the granite is interpreted to be  $182 \pm 4$  Ma.

#### **BO-59 K-feldspar biotite granite, West side batholith above new airport**

This sample gave a very low zircon yield. There are mixed grain shapes and sizes (50-200  $\mu\text{m}$ ), all with relict igneous shape and zoning. There is planar and oscillatory zoning visible in most grains. Seven analyses form a sub-concordant population at  $166 \pm 2/4$  Ma (MSWD = 1.2) (Fig. 12). Two grains are older at ca. 206 Ma; these are not from obviously older cores, but still may represent inheritance.

Allanite exhibits an array with a high common lead content, and probable mixing between two events. A cluster of analyses at the oldest ages produces a regression with an age of ca. 166 Ma that is correlative to the oldest zircon population. Regression through the younger analysis gives a lower intercept of ca. 18 Ma, providing a maximum age for a young allanite growth or resetting. The age of granite crystallisation is interpreted to be  $166 \pm 4$  Ma, and ca. 18 Ma is interpreted as a tectonothermal event affecting this unit.

### **BO-62 Biotite monzogranite, middle of batholith**

This sample gave a moderate zircon yield (Fig. 13). There are mixed grain sizes and shapes from 50 to 200  $\mu\text{m}$ . Most grains have oscillatory or planar igneous zoning, but this is disturbed or recrystallized in many cases. Inclusions are fairly common. Some grains have faint zoning that looks disturbed. Thick rim overgrowths occur on some grains. In total, 137 analyses were obtained from 80 grains. The majority of the analyses fall on a regression (mixing line) between ca. 800 Ma and a young (Neogene) lower intercept. Scrutiny of the younger ages and lower intercept, reveals two distinct sub-concordant populations. One is dated at ca. 14 Ma, obtained from 4 grains, and some with oscillatory zoning. Another is dated at ca. 5 to 6 Ma. Overlapping ages of ca. 6.3 Ma across one grain, 6.7 Ma across another, and 5 to 5.5 Ma in others, implies prolonged or multiple crystallisation event/s. Discordance in many analyses can be attributed to a high common lead content for many of the young analyses. The youngest age population, with concordant (>90%) analyses ranging from 5.0 to 6.7 Ma, are derived from recrystallised zones, embayed but oscillatory zoned rims and overgrowths, and one primary oscillatory zoned crystal. Additionally, multiple overlapping ages have been determined from single crystals. Collectively, the data imply that the young ages are attributable to crystallisation in a melt, rather than being a result of age disturbance/resetting.

One allanite analyses with moderate radiogenic lead content gives an age of ca. 170 Ma (with an assumed common lead composition). Since this may be disturbed, no particular emphasis should be placed on this age; however, it is interesting to note that it correlates with zircon and allanite ages from other samples. A population of allanite analyses with very high common lead content define a poor regression to a young age; the lower intercept is  $5 \pm 1/1$  Ma. This age and uncertainty should be given low

confidence, since there is very little radiogenic component; however, it is also interesting to note that it correlates with the youngest zircon age domains at ca. 5 Ma.

#### **BO-68 Garnet Two-mica leucogranite, Yanzigou valley**

This sample gave a moderate zircon yield. The sample comprises elongate igneous grains with broken tips that are 100 to 300  $\mu\text{m}$  long. All are oscillatory or planar zoned, but many are also recrystallized along internal zones. It mostly appears there is one growth phase, with no obvious rim overgrowths. A couple of presumably inherited grains give ages of ca. 531 Ma and 685 Ma. The rest of the analyses cluster around a possible single population, with lead-loss recorded in a few grains, and a couple of analyses possibly representing slightly older inheritance. Twenty sub-concordant analyses give an age of  $204 \pm 2/4$  Ma (MSWD = 1.4) which is interpreted as the age of granite crystallisation (Fig. 14). One concordant analysis at 177 Ma is from a bright rim, suggesting a younger tectonothermal event at this age is recorded in this sample.

Four allanite analyses give an age of ca. 173 Ma; this correlates with the single rim age of 177 Ma, adding confidence to the interpretation of a separate event younger than 205 Ma.

#### **BO-76 Foliated biotite hornblende granodiorite, Yanzigou**

This sample gave a moderate zircon yield, with elongate grains that are 100 to 300  $\mu\text{m}$  long. Zoning is oscillatory, planar or sector, and is typically quite weak in contrast (in CL). Inclusions and fractures are common, and some grains appear to have resorption features. Rim-type overgrowths are not apparent, but some outer zones may be recrystallized. Despite the appearance of potentially different growth zones, thirty-two analyses define a single population at  $215 \pm 2/5$  Ma (MSWD = 1.3) which is interpreted as the age of granite crystallisation (Fig. 15). The only exclusion is a single older, and presumably inherited grain (discordant  $^{207}\text{Pb}/^{206}\text{Pb}$  age of 790 Ma. A population of moderately radiogenic allanite analyses gives an apparent regression, with minimal scatter, at ca. 205 Ma. A population of moderately radiogenic titanite analyses gives a regression with an overlapping age of ca. 206 Ma; three analyses are younger, and may reflect open-system disturbance, lead-loss, or younger titanite growth.

### Summary and interpretation of age data

The age data from the seven samples described above constrain two striking tectonic-plutonic events: a complex Triassic-Jurassic (Indosinian) plutonic record, and a possible Eocene to Miocene record of monzonite-leucogranite emplacement (Fig. 16). The Indosinian events are recorded in six of the seven samples. Discrete zircon populations in five of these samples, including those interpreted as inherited, probably document a series of igneous crystallization events, at ca. 215, 204, 182, 166 and 159 Ma. For those samples that have Indosinian crystallisation ages, inherited zircons are few, with ages ranging from ca. 200 Ma to 2469 Ma, but with the dominant subset being Neoproterozoic. Indosinian-aged inheritance, for example 206 Ma grains in a 166 Ma monzogranite, suggests reworking of young material during the complex Indosinian evolution. Allanite ages which are younger than the main zircon population, but also of Indosinian age, imply that younger Indosinian tectonothermal events or intrusions affected older Indosinian magmatic rocks. One sample (BO62) lacks any Indosinian record in its zircon age data, but includes many ca. 800 Ma analyses, mostly from zircon cores. The lack of inherited zircons in most samples precludes a confident derivation of the magmatic source based on age characteristics. Neoproterozoic ages are common in the Triassic Songpan-Ganze sediments, which are likely source rocks for the (S-type) leucogranites. The ca. 800 Ma Kangding gneiss complex (Zhou et al., 2002) may have sourced the 800 Ma cores in BO62, either directly (i.e. through melting), or indirectly via erosion of the complex and melting of the resulting sedimentary rocks.

Young melt events are recorded in three samples. BO62 has zircon overgrowths on ca. 800 Ma cores, with concordant analyses implying two separate ages of new zircon growth, one at ca. 15 Ma, and one at ca. 5 Ma. A poor allanite regression giving a ca. 5 Ma age supports this younger age. Migmatization in one sample (BO52) is presumed to be at least as young as the three youngest zircon ages at ca. 51 Ma and 35 Ma. Allanite at ca. 16 Ma may represent the timing of migmatization. A cross-cutting pegmatite (BO55) has a small population of sub-concordant zircon analyses at ca. 41-37 Ma suggesting a possible growth event at this time. Younger analyses are scattered, but imply pegmatite crystallisation at ca. 15 Ma, constrained by the youngest concordant analyses.

The U-Pb age data presented above leads to the following key question: how much young (i.e. Miocene) melting has occurred in the Gongga Shan batholith and is

recorded in its composite tectono-magmatic history? Oscillatory zoned (in CL) overgrowths of variable thickness, and with resorption textures, suggest that both ca. 16-14 Ma and 5 Ma events involved significant melt at the grain-scale. The sample that contains zircons of both these ages (BO 62) is an undeformed biotite monzogranite that, from our field observations and mapping, represents a volumetrically significant part of the batholith in its central region. This would imply that significant portions of the batholith are as young as 5 Ma. Although there is no outcrop evidence anywhere in East Tibet for any regional metamorphism or crustal thickening at this time, this may be a function of erosion and exposure level and it is possible that these rocks remain buried.

Previous U-Pb age constraints from different parts of the batholiths reveal ages from ca. 35 Ma to 13 Ma (Roger et al., 1995; Li and Zhang, 2013). The 14 Ma age obtained here for zircon growth overlaps with these previous ages. Li and Zhang (2013) found ages of ca. 32 to 37 Ma in migmatitic rocks, which they interpret as a high-temperature event at this time. The 41 to 37 Ma ages in BO55 are potentially recording part of this same cryptic event.

## **DISCUSSION AND CONCLUSIONS**

### **Gongga Shan batholith**

The Gongga Shan massif is a composite granite batholith composed of three distinct parts. Much of the batholith appears to be of Indosinian origin. Triassic-Jurassic I-type granodiorite-biotite granite (215 – 159 Ma) formed in an Andean-type setting during closure of PalaeoTethys. Some volumetrically unknown component is composed of a garnet two-mica leucogranite of crustal melt origin but also of Indosinian age ( $204 \pm 2$  Ma). A third component is a multiple injection complex that exhibits ages from 41 to 15 Ma, with leucogranites and a pegmatite dyke network that intruded between 15 – 5 Ma. Ductile fabrics within the granites and migmatites show flow folding related to middle or lower crust melting processes and thus are not related to the Xianshui-he strike-slip fault. Several samples show evidence of old Indosinian and young crustal melts in the same rock. The young leucogranites may have formed by re-melting of Indosinian crust, possibly buried components of the Songpan-Ganze flysch. Since much of the batholith is inaccessible and remains

undated, it is unclear precisely what proportion of the batholith is composed of young Miocene granite.

### **Evidence for young Cenozoic partial melting**

Only a few areas across Tibet show evidence for localised young crustal melts. Certainly the exposed geology of eastern Tibet consists of old, Precambrian basement complexes (e.g. Kangding complex), Palaeozoic – early Mesozoic (meta-)sedimentary rocks and Palaeozoic-Triassic granites. The young granitic phase of the Gongga Shan batholith (Roger et al., 1995; Li and Zhang, 2013; this paper) is the only evidence for Late Miocene or younger crustal melting in this part of Tibet. Like the Himalayan leucogranites, these young S-type granites are derived by dominantly muscovite-dehydration reactions in pelitic protoliths in the middle crust. Similar young granites are reported from the Western Nyenchen Tanggla range of south Tibet where U-Pb zircon ages of 25-8 Ma have been obtained (Liu et al., 2004; Kapp et al., 2005; Weller et al., 2016). These young melts are thought to represent an exhumed partial melt, similar to the small ‘bright spots’ imaged on seismic and magnetotelluric studies (Nelson et al., 1996; Brown et al., 1996; Bai et al., 2010). We suggest that the young granite phases of Gongga Shan may have a similar provenance. The limited amount of young crustal melt and the lack of regional Cenozoic metamorphism precludes any channel flow operating in eastern Tibet, unlike the south Tibet-Himalayan mid-crustal channel flow.

### **Xianshui-he Fault**

All the granites in the Gongga Shan batholith are cut abruptly by the left-lateral Xianshui-he fault. The NW continuation of the Xianshui-he fault, called the Garze-Yushu fault shows major offsets of tributary rivers of the Yangtze and has suffered numerous earthquakes in the past few hundred years, including the 2010 Mw 6.8 Yushu event (Li et al., 2011). The Jinsha river course appears to have been offset by ~85 km and the course of the Yalong river offset by 35 km (Wang et al., 1998). The fault shows maximum sinistral offsets of ~85 km in offset river courses of the Jinsha and upper Yangtze rivers (Fig. 17). These fault strands each show only minor (5-10 km) offsets of the granite margin. A major transpressional component is present along the Kangding – Moxi segment accounting for the 2-3 km of differential topography in the Gongga Shan region. The fault system also curves around from

WNW-ESE (Ganzi-Yushu fault) to NW-SE (Xianshui-he fault) to N-S (Anninghe fault) showing almost 90° anticlockwise rotation of the Lhasa and Qiangtang blocks, associated with the northward indentation of India to the west. Our data suggests that the Xianshui-he fault was initiated <5 Ma because it cuts granites of that age. It is theoretically possible that the fault has an earlier history but there is no record of this in the present-day exposures. Ductile fabrics in parts of the injection complex along the eastern margin of the batholith are abruptly truncated by vertical brittle strike-slip fault strands along the Kangding road section. Further south the Xianshui-he fault is ~10 km or more east of the batholith. The granites are not connected to the strike-slip fault in any way and their ages relate to localised crustal melting, not to strike-slip faulting. Measured GPS slip rates suggest present day slip may be ~10-12 mm/yr (Zhang et al., 2004). Despite being one of the most seismically active faults in Tibet, it shows only limited offset and therefore cannot have been responsible for large amounts of eastward lateral extrusion of the thickened crust.

### **Composition of the lower crust beneath eastern Tibet**

Do the Gongga Shan granites represent melts derived from the lower crust of Eastern Tibet? It is possible that the young crustal melts seen in Gongga Shan are representative of widespread young crustal melting, or that they are volumetrically minor melts sourced from the middle crust. The Longmen Shan and Lijiang faults mark a major transition from seismically fast (cratonic) mantle to the east (Sichuan basin, southern Yunnan and Yangtze craton) and seismically low wave speeds to the west in the Tibetan plateau (Liu et al., 2014). We suggest that this Longmen Shan – Lijiang fault system as well as bounding the topographically high plateau to the west, marks the eastern boundary of the indenting Indian plate lower crust. We suggest that the lower crust of the Lhasa and Qiangtang terranes are both underlain by strong, Archean-Palaeoproterozoic crust of India underthrusting the plateau north as far as the Xianshui-he fault. The crust to the southwest of the Xianshui-he fault shows low-velocity zones in the mid-crust, radial anisotropy and higher electrical conductivity consistent with localised pockets of melt (Huang et al., 2010; Bai et al., 2010). The crust north of the Xianshui-he fault is subtly different showing higher average viscosity (Liu et al., 2014). The fact that Precambrian basement, Palaeozoic cover rocks and Indosinian metamorphic rocks (Danba area) are exposed at the surface in eastern Tibet above 65-70 km thick crust, coupled with the lack of Cenozoic

metamorphism or deformation suggests that the Tibetan crust has been passively uplifted by underthrusting of Indian basement beneath (Argand, 1924; Searle et al., 2011).

### **Lower crustal flow beneath eastern Tibet?**

Although some geophysical data points to a weak middle crust with pockets of inter-connected fluids (Mechie and Kind, 2013), there is no geological evidence anywhere for lower crustal flow (Royden et al., 1997; Clark and Royden, 2000). Unlike south Tibet-Himalaya, the minor amount of fluids in the middle crust in eastern Tibet is not sufficient to form any sort of lateral channel-type flow, and there is no evidence along the Longmen Shan range of Cenozoic metamorphism or east-vergent ductile flow deformation. Along the Himalaya there is abundant evidence for mid-crustal channel flow during the Miocene (10-20 km thickness of partially molten middle crust migmatites and garnet, two-mica ( $\pm$  cordierite, andalusite, sillimanite) leucogranites bounded by a south-vergent thrust below and a north-dipping low-angle normal fault above; Searle et al., 2010b), but along the eastern border of Tibet, the Longmen Shan, the geology and structure is completely different. Here, the deformation, metamorphism and magmatism is almost entirely Triassic-Jurassic (Weller et al., 2013; this paper) or older. There is no evidence for Cenozoic crustal shortening, and no evidence for east-directed thrusting or flow of any sort. If the lower crust beneath Tibet was flowing to the east as suggested by Royden et al. (1997, 2008) and Clark and Royden (2000), then there should be a large amount of Cenozoic-active shortening in the upper crust. There is none, only the steep west-dipping thrust faults associated with the M-7.9 Wenchuan earthquake accommodating minor active shortening (Hubbard and Shaw, 2009). If lower crustal flow had occurred, the geology of southern Yunnan would be expected to show this. Instead the proposed 'flow' directions cut across geological strike and structures throughout Yunnan. We propose, instead of outward flow, extensional tectonics and lowering of surface elevation (Royden et al., 1997, 2008) that the plateau is maintaining or even increasing elevation as evidenced by compressional tectonics along the southern margin (Himalaya-south Tibet) and compressional tectonics along the LongMen shan (Wenchuan earthquake).

The more reasonable model to explain the geology of eastern Tibet is one of passive underthrusting of Indian lower crust towards the NNE all the way northward

as far as the Xianshui-he fault. At the time of India-Asia collision and closure of NeoTethys, ~50 m.y. ago, the north Indian plate consisted of ca 7-8 km of Phanerozoic upper crustal sediments overlying 2-4 km thickness of Neoproterozoic low-grade sedimentary rocks (Haimanta-Cheka Groups), overlying 25-30 km of Archean - Palaeoproterozoic granulite basement (Indian Shield). The Himalaya are comprised entirely of Neoproterozoic and younger rocks, mainly unmetamorphosed in the Tethyan Himalaya upper crust, and metamorphosed in the Greater Himalaya middle crust, structurally below the Tethyan Himalaya. At least 500 km, probably more like 1000 km, of upper crustal shortening has occurred since collision in the Indian Himalaya. The Archean granulite lower crust that originally underlay these rocks was old, cold and dry, and thus un-subductable. The only place this Indian lower crust could have gone is northward, underthrusting the Asian plate beneath the Lhasa and Qiangtang blocks of Tibet in a process originally suggested by Argand (1924). We suggest that this underthrusting Indian lower crust effectively doubled the Tibetan crust since 50 Ma and passively uplifted the rocks of the Tibetan plateau. This alone can account for the almost complete lack of Cenozoic shortening and Cenozoic metamorphism across the Tibetan plateau. Our Late Miocene ages from the Gongga Shan granites are the only indication of post-collision Cenozoic metamorphism and magmatism in Eastern Tibet, but are volumetrically minor.

### **Acknowledgements**

We thank Ministry of Science and Technology, Taiwan and the National Natural Science Foundation, of China for support and funding. Landsat-7 imagery and SRTM DEMs are courtesy of NASA. Fieldwork was funded mainly by the Institute of Geology, China Earthquake Administration, Beijing. Searle and Chung were partially supported by a Taiwan-UK Royal Society grant. U-Pb dating was carried out at the NERC (UK) laboratory at the British Geological Survey, Keyworth. Elliott and Weller were supported by NERC grants. St-Onge was funded by the Earth Sciences Sector, Natural Resources Canada. We thank Nicole Rayner (GSC), two anonymous reviewers and Associate Editor Mike Taylor for detailed comments that significantly improved the manuscript. This is GSC Earth Sciences Sector contribution number 20150332.

## REFERENCES

- Allen, C. R., Zhuoli, L., Hong, Q., Xueze, W., Huawei, Z. & Weishi, H., 1991, Field study of a highly active fault zone: The Xianshuihe fault of southwestern China: *GSA Bulletin*, v. 103, p. 1178-1199, doi: 10.1130/0016-7606(1991)103<1178:FSOAHA>2.3.CO;2.
- Argand, E., 1924, Le tectonique de l'Asie: Proc. 13<sup>th</sup> International Geological Congress, v. 7, p. 171-372.
- Bai, D. et al., 2010, Crustal deformation of the eastern Tibetan plateau revealed by magnetotelluric imaging: *Nature Geosciences*, v. 3, p. 358-362.
- Burchfiel, B. C., Deng, Q., Molnar, P., Royden, L., Wang, Y., Zhang, P. and Zhang, W. 1989, Intracrustal detachment within zones of continental deformation: *Geology*, v. 17, p. 748-751.
- Burchfiel, B.C., Zhang, P., Wang, Y. and 5 others, 1991, Geology of the Haiyuan Fault zone, Ningxia-Hui autonomous region, China, and its relation to the evolution of the Northeast margin of the Tibetan Plateau: *Tectonics*, v. 10, p. 1091-1110.
- Burchfiel, B.C. and Chen, Ziliang, 2010, Tectonics of the Southeastern Tibetan Plateau and its adjacent foreland: *Geological Society of America Memoir*, v. 210, 231p.
- Chan, G.H-N., Waters, D.J., Searle, M.P., Aitchison, J.C., Horstwood, M.S.A., Crowley, Q., Lo, C-H. and Chan, J.S-L., 2009, Probing the basement of southern Tibet: evidence from crustal xenoliths entrained in a Miocene ultrapotassic dyke: *Journal of the Geological Society London*, v. 166, p. 45-52.
- Chiu, H-Y., Chung, S-L., Wu, F-Y. and 7 others, 2009, Zircon U-Pb and Hf isotopic constraints from eastern Transhimalayan batholiths on the precollisional magmatic and tectonic evolution in southern Tibet: *Tectonophysics*, doi: 10.1016/j.tecto.2009.02.034.
- Chu, M-F., Chung, S-L, Song, B. and 5 others., 2006, Zircon U-Pb and Hf isotope constraints on the Mesozoic tectonics and crustal evolution of southern Tibet: *Geology*, v. 34, no. 9, p. 745-748.
- Chung, S-L., Lo, C-H., Lee, T-Y., Zhang, Y., Xie, Y., Li, X., Wang, K-L. and Wang, P-L., 1998, Diachronous uplift of the Tibetan Plateau starting 40 Myr ago: *Nature*, v. 394, p. 769-773.
- Chung, S-L., Liu D., Ji, J. and 7 others, 2003, Adakites from continental collision zones: Melting of thickened lower crust beneath southern Tibet: *Geology*, v. 31, no. 11, p. 1021-1024.
- Chung, S-L., Chu, M-F., Zhang, Y. and 7 others., 2005, Tibetan tectonic evolution inferred from spatial and temporal variations in post-collisional magmatism: *Earth Science Reviews*, v. 68, p. 173-196.
- Chung, S-L., Chu, M-F., Ji, J. and 5 others., 2009, The nature and timing of crustal thickening in Southern Tibet: Geochemical and zircon Hf isotopic constraints from post-collisional adakites: *Tectonophysics*, v. 477, p. 36-48.

- Clark, M.K. and Royden, L.H., 2000, Topographic ooze: Building the eastern margin of Tibet by lower crustal flow: *Geology*, v. 28, p. 703-706.
- Dewey, J. and Burke, K., 1973, Tibetan, Variscan and Precambrian basement reactivation: Products of a continental collision: *Journal of Geology*, v. 81, p. 683-692.
- Ding, L., Kapp, P., Yue, Y. and Lai, Q., 2007, Postcollisional calc-alkaline lavas and xenoliths from the southern Qiangtang terrane, central Tibet: *Earth and Planetary Science Letters*, v. 254, p. 28-38.
- Elliott, J.R., Biggs, J., Parsons, B. and Wright, T.J., 2008, InSAR slip rate determination on the Altyn Tagh fault, northern Tibet, in the presence of tomographically correlated atmospheric delays: *Geophysical Research Letters*, v. 35, L12309, doi:10.1029/2008GL033659
- England, P. and Molnar, P., 1990, Right-lateral shear and rotation as the explanation for strike-slip faulting in east Tibet: *Nature*, v. 344, p. 140-142.
- Gan, W., Zhang, P., Shen, Z.-K., Niu, Z., Wang, M., Wan, Y., Zhou, D. and Cheng, J., 2007, Present-day crustal motion within the Tibetan Plateau inferred from GPS measurements: *Journal of Geophysical Research*, v. 112, B08416, doi:10.1029/2005JB004120
- Green, O.R., Searle, M.P., Corfield, R.I. and Corfield, R.M., 2008, Cretaceous-Tertiary carbonate platform evolution and the age of the India-Asia collision along the Ladakh Himalaya (Northwest India): *Journal of Geology*, v. 116, p. 331-353.
- Hacker, B., Gnos, E., Ratschbacher, L. and 5 others, 2000, Hot and dry deep crustal xenoliths from Tibet: *Science*, v. 287, p. 2463-2466.
- Harrowfield, M.J. and Wilson, C.J.L., 2005, Indosinian deformation of the Songpan-Garze fold belt, northeastern Tibetan plateau: *Journal of Structural Geology*, v. 27, p. 101-117.
- Hetzl, R., Niedermann, S. et al., 2002, Low slip rates and long-term preservation of geomorphic features in Central Asia: *Nature*, v. 417, p. 428-432.
- Haines, S.S., Klempner, S.L., Brown, L., Jingru, G., Mechie, J., Meissner, Ross, A. and Wenjin, Z., 2003, INDEPTH III seismic data: From surface observations to deep crustal processes in Tibet: *Tectonics*, v. 22, doi: 10.1029/2001TC001305
- Hetényi, G., Cattin, R., Brunet, F., Bollinger, L., Vergne, J., Nabelek, J.L. and Diamant, M., 2007, Density distribution of the India plate beneath the Tibetan Plateau: Geophysical and petrological constraints on the kinetics of lower crustal eclogitization: *Earth and Planetary Science Letters*, v. 264, p. 226-244.
- Horstwood, M. S., Foster, G. L., Parrish, R. R., Noble, S. R., and Nowell, G. M. (2003), Common-Pb corrected in situ U–Pb accessory mineral geochronology by LA-MC-ICP-MS. *Journal of Analytical Atomic Spectrometry*, v. 18(8), p. 837-846.
- Houseman, G., McKenzie, D. and Molnar, P., 1981, Convective instability of a thickened boundary layer and its relevance for thermal evolution of continental convergent belts: *Journal of Geophysical Research*, v. 86, p. 6115-6132.

- Huang, H., Yao, H. and van der Hilst, R.D., 2010, Radial anisotropy in the crust of SE Tibet and SW China from ambient noise interferometry: *Geophysical Research Letters*, v. 37, doi: L21310
- Hubbard, J. and Shaw, J.H., 2009, Uplift of the LongMen shan and Tibetan Plateau and the 2008 Wenchuan earthquake: *Nature*, v. 458, p. 194-197.
- Kapp, P., Yin, A., Harrison, T.M. and Ding, L., 2005, Cretaceous-Tertiary shortening, basin development and volcanism in central Tibet: *Geological Society America Bulletin*, v. 117, p. 865-878.
- Kapp, P., DeCelles, P.G., Gehrels, G., Heizler, M. and Ding, L., 2007, Geological records of the Lhasa-Qiangtang and Indo-Asian collisions in the Nima area of central Tibet: *Geological Society America Bulletin*, v. 119, p. 917-932.
- Kapp, P., DeCelles, P.G., Leier, A.L., Fabijanic, J.M., He, S., Pullen A., Gehrels, G. and Ding, L., 2007b, The Gangdese retroarc thrust belt revealed: *GSA Today*, v. 17, p. 4-9, doi:10.1130/GSAT01707A.1.
- Kirby, E., Reiners, P.W., Krol, M.A., Hodges, K.V., Whipple, K.X., Farley, K.A., Chen, Z. and Tang, W., 2002, Late Cenozoic evolution of the eastern margin of the Tibetan Plateau: Inferences from  $^{40}\text{Ar}/^{39}\text{Ar}$  and (U-Th)/He thermochronology: *Tectonics*, v. 21, TC1001, doi: 10.1029/2000TC001246
- Lee, H-Y, Chung, S-L., Lo, C-H., Ji, J., Lee, T-Y., Qian, Q. and Zhang, Q., 2009, Eocene Neotethyan slab breakoff in southern Tibet inferred from the Linzizong volcanic record: *Tectonophysics*, v. 477, p. 20-35.
- Leier, A.L., DeCelles, P.G., Kapp, P. and Ding, L. 2007. The Takena Formation of the Lhasa terrane, southern Tibet: record of a Late Cretaceous retroarc foreland basin: *Geological Society of America Bulletin*, v. 119, p. 31-48.
- Liang, X., Sandvol, E., Chen, Y., Hearn, T., Ni, J., Klemperer, S., Shen, Y., and Tilmann, F., 2012, A complex Tibetan upper mantle: a fragmented Indian slab and no south-verging subduction of Eurasian lithosphere: *Earth and Planetary Science Letters*, v. 333, p. 101-111 doi:10.1016/j.epsl.2012.03.036
- Li Hailong and Zhang, Yueqiao, 2013, Zircon U-Pb geochronology of the Kongga granitoid and migmatite: Constraints on the Oligo-Miocene tectono-thermal evolution of the Xianshuihe fault zone, East Tibet: *Tectonophysics*, v. 606, p. 127-139.
- Li, Z., Elliott, J.R., Feng, W., Jackson, J.A., Parsons, B.E. and Walters, R.J., 2011, The 2010 Mw 6.8 Yushu (Qinhai, China) Earthquake: constraints provided by InSAR and Body Wave Seismology: *Journal of Geophysical Research*, v. 116, doi:10.1029/2011JB008358
- Liu, Q., van der Hilst, R.D., et al., 2014, Eastward expansion of the Tibetan Plateau by crustal flow and strain partitioning across faults: *Nature Geoscience*, v. 7, 10.1038/NCEO2130
- Liu, S. W., Wang, Z. Q., Yan, Q. R., Li, Q. G., Zhang, D. H., & Wang, J. G., 2006, Timing, petrogenesis and geodynamic significance of Zheduoshan Granitoids: *Acta Petrologica Sinica*, v. 22, p. 343-352.
- Ludwig, K. R., 2003. *User's manual for Isoplot 3.00: a geochronological toolkit for Microsoft Excel* (No. 4). Kenneth R. Ludwig.

McKenna, L.W. and Walker, J.D., 1990, Geochemistry of crustally derived leucocratic igneous rocks from the Ulugh Muztagh area, Northern Tibet and their implications for the formation of the Tibetan Plateau: *Journal of Geophysical Research*, 95, 21483-502.

Mechie, J. and Kind, R., 2013, A model of the crust and mantle structure down to 700 km depth beneath the Lhasa to Golmud transect across the Tibetan Plateau as derived from seismological data: *Tectonophysics*, v. 606, p. 187-197/

Molnar, P. and Tapponnier, P., 1975, Cenozoic tectonics of Asia: Effects of a continental collision: *Science*, v. 189, p. 419.

Molnar, P. and Tapponnier, P., 1978, Active tectonics of Tibet: *Journal of Geophysical Research*, v. 83, p. 5361.

Molnar, P., Burchfiel, B.C., Ziyun, Z., K'Uangyi, L., Shuji, W. and Minmin, H., 1987, Geologic evolution of Northern Tibet: results from an expedition to Ulugh Muztagh: *Science*, v. 235, p. 299-305.

Molnar, P., England, P.C. and Martinod, J., 1993, Mantle dynamics, uplift of the Tibetan Plateau and the Indian monsoon: *Reviews of Geophysics*, v. 31, p. 357-396.

Nábelek, J., Hetényi, G. and the HiCLIMB team, 2009, Underplating in the Himalaya-Tibet collision zone revealed by the Hi-CLIMB experiment: *Science*, v. 325, p. 1371-1374.

Nelson, K.D., Zhao, W., Brown, L.D. and 25 others., 1996, Partially molten middle crust beneath Southern Tibet: Synthesis of Project INDEPTH results: *Science*, v. 274, p. 1684- 1688.

Peltzer, G. and Tapponnier, P., 1988, Formation and evolution of strike-slip faults, rifts and basins during the India-Asia collision: an experimental approach: *Journal of Geophysical Research*, v. 93, p. 15085-15117.

Peltzer, G., Tapponnier, P. and Armijo, R., 1989, Magnitude of late Quaternary left-lateral displacements along the north edge of Tibet: *Science*, v. 246, p. 1285-1289, doi:10.1126/science.246.4935.1285

Prestley, K., Jackson, J. and McKenzie, D., 2008, Lithospheric structure and deep earthquakes beneath India, the Himalaya and southern Tibet: *Geophysical Journal International*, v. 172, p. 345-362.

Ritts, B.D. and Biffi, U., 2000, Magnitude of post-Middle Jurassic (Bajocian) displacement on the central Altyn Tagh fault system, northwest China: *Geological Society of America Bulletin*, v. 112 (1), p. 61-74, doi:10.1130/0016-7606(2000)112<61:MOPJBD>2.0.CO;2.

Roger, F., Calassou, S., Lancelot, J., Malavielle, J., Mattauer, M., Zhiqin, X. Ziwen, H. and Liwei, H., 1995, Miocene emplacement and deformation of the Konga Shan granite (Xianshui He fault zone, west Sichuan, China): Geodynamic implications. *Earth and Planetary Science Letters*, v. 130, p. 201-216.

Roger, F., Arnaud, N., Gilder, S., Tapponnier, P., Jolivet, M., Brunel, M., Malavielle, J. and Xu, Z., 2003, Geochronological and geochemical constraints on Mesozoic suturing in East Central Tibet: *Tectonics*, v. 22 (4), p. 1037 doi:10.1029/2002TC001466

- Roger, F., Malavielle, J., Leloup, H., Calassou, S. and Xu, Z., 2004, Timing of granite emplacement and cooling in the Songpan-Garze fold belt (eastern Tibetan plateau) with tectonic implications: *Journal of Asian Earth Sciences*, v. 22, p. 465-481.
- Roger, F., Jolivet, M. and Malavielle, J., 2010, The tectonic evolution of the Songpan-Garze (North Tibet) and adjacent areas from Proterozoic to present: A synthesis: *Journal of Asian Earth Sciences*, v. 39, p. 254-269.
- Royden, L.H., Burchfiel, B.C., King, R.W., Wang, E., Chen, Z., Shen, F. and Liu, Y., 1997, Surface deformation and lower crust flow in Eastern Tibet: *Science*, v. 276, p. 788-790.
- Royden, L.H., Burchfiel, B.C., and van der Hilst, R.D., 2008. The geological evolution of the Tibetan Plateau: *Science*, v. 321, p. 1054-1058.
- Schulte-Pelkum, V., Mondalve, G. Sheehan, A., Pandey, M.R., Sapkota, S., Bilham, R. and Wu, F., 2005, Imaging the Indian subcontinent beneath the Himalaya: *Nature*, v. 435, p. 1222-1225.
- Searle, M.P., Parrish, R.R., Thow, A.V., Noble, S.R., Phillips, R.J. and Waters, D.J. 2010a, Anatomy, age and evolution of a collisional mountain belt: the Baltoro granite batholith and Karakoram Metamorphic complex, Pakistani Karakoram. *Journal of the Geological Society, London*, v. 167, p. 183-202. doi: 10.1144/0016-76492009-043
- Searle, M.P., Cottle, J.M., Streule, M.J. and Waters, D.J., 2010b, Crustal melt granites and migmatites along the Himalaya: melt source, segregation, transport and granite emplacement mechanisms: *Transactions of the Royal Society of Edinburgh*, v. 100, p. 219-233. doi:10.1017/S175569100901617X
- Searle, M.P., Yeh, M-H., Lin, T-H. and Chung, S-L., 2010c, Structural constraints on the timing of left-lateral shear along the Red River shear zone in the Ailao Shan and Diancang Shan Ranges, Yunnan, Southwest China: *Geosphere*, v. 6 (4), p. 1-23. doi: 10:1130/GES00580.1
- Searle, M.P., Elliott, J.R., Phillips, R.J. and Chung, S-L., 2011, Crustal – lithospheric structure and continental extrusion of Tibet: *Journal of Geological Society, London*, v. 168, p. 633-672, doi:10.1144/0016-76492010-139
- Sengör, A.M.C., 1985, East Asian tectonic collage: *Nature*, v. 318, p. 15-17.
- Shapiro, N.M., Ritzwoller, M.H., Molnar, P. and Levin, V., 2004, Thinning and flow of Tibetan crust constrained by seismic anisotropy: *Science*, v. 305, p. 233-236.
- Shen, Z.K., Wang, M, Li, X.Y., Jackson, D.D. Yin, A., Dong, D.N. and Fang, P., 2001, Crustal deformation along the Altyn Tagh fault system, western China from GPS: *Journal of Geophysical Research*, v. 106, p. 30607-621.
- Shen, Z.-K., Lu, J., Wang, M. and Burgmann, R., 2005, Contemporary crustal deformation around the southeast borderland of the Tibetan Plateau: *Journal of Geophysical Research*, v. 110, doi: [10.1029/2004JB003421](https://doi.org/10.1029/2004JB003421)
- Sichuan Bureau of Geology and Mineral Resources, 1981, Sichuan Geological Map series, scale 1: 200,000; Chengdu, Sichuan, China.
- Sláma, J., Košler, J., Condon, D. J., Crowley, J. L., Gerdes, A., Hanchar, J. M., Horstwood, M. S. A., Morris, G. A., Nasdala, L., Norberg, N., Schaltegger, U., Schoene, B., Tubrett, M. N., and Whitehouse, M. J., 2008, Plešovice zircon—a new

- natural reference material for U–Pb and Hf isotopic microanalysis: *Chemical Geology*, v. 249, p. 1-35.
- Smye, A. J., Roberts, N. M., Condon, D. J., Horstwood, M. S., & Parrish, R. R. 2014. Characterising the U–Th–Pb systematics of allanite by ID and LA-ICPMS: Implications for geochronology: *Geochimica et Cosmochimica Acta*, v.135, p. 1-28.
- Sol, S., Meltzer, A., Burgman, R. and 10 others, 2010, Geodynamics of the southeastern Tibetan Plateau from seismic anisotropy: *Geology*, v. 35, p. 563-566.
- Spencer, C.J., Roberts, N.M.W., Cawood, P.A., Hawkesworth, C.J., Prave, A.R., Antonini, A.S.M., Horstwood, M.S.A., and E.I.M.F., 2014, Intermontane basins and bimodal volcanism at the onset of the Sveconorwegian Orogeny, southern Norway: *Precambrian Research*, v. 252, p. 107-118.
- St-Onge, M.R., Rayner, N. and Searle, M.P., 2010, Zircon age determinations for the Ladakh batholith at Chumatang (Northwest India): Implication for the age of the India-Asia collision in the Ladakh Himalaya: *Tectonophysics*, v. 495, p. 171-183.
- Stacey, J. T., & Kramers, J. D., 1975, Approximation of terrestrial lead isotope evolution by a two-stage model. *Earth and Planetary Science Letters*, v. 26, p. 207-221.
- Tapponnier, P. and Molnar, P., 1977, Active faulting and tectonics in China: *Journal of Geophysical Research*, 82, 2905-2930.
- Tapponnier, P., Peltzer, G., Ledain, A.Y., Armijo, R., and Cobbold, P.R., 1982, Propagating extrusion tectonics in Asia: New insights from simple experiments with plasticine: *Geology*, v. 10, p. 611-616.
- Tapponnier, P., Zhiqin, X., Roger, F., Meyer, B., Arnaud, N., Wittlinger, G. and Yang, J., 2001, Oblique stepwise rise and growth of the Tibet Plateau: *Science*, v. 294, p. 1671-1677.
- Taylor, M. and Yin, A., 2009, Active structures of the Himalaya-Tibet orogeny and their relationships to earthquake distribution, contemporary strain field and Cenozoic volcanism: *Geosphere*, p. 199-214, doi:10.1130/GES00217.1
- Tilmann, F., Ni, J. and INDEPTH III Seismic team, 2003, Seismic imaging of the downwelling Indian lithosphere beneath Central Tibet: *Science*, v. 300, p. 1424-1427.
- Wang, E., Burchfiel, B.C., Royden, L.H., Liangzhong, C., Jishen, C., Wenxin, L. and Zhiliang, C., 1998, Late Cenozoic Xianshuihe-Xiaojiang, Red River, and Dali Fault systems of southwestern Sichuan and Central Yunnan, China: *Geological Society of America Special Paper*, v. 327, p. 1-108.
- Wang, E., Meng, K., Su, Z., Meng, Q., Chu, J., Chen, Z., Wang, G., Shi, X. and Liang, X., 2014, Block rotation: Tectonic response of the Sichuan basin to the southeastward growth of the Tibetan Plateau along the Xianshuihe-Xiaojiang fault. *Tectonics*, v. 33, p. 686-717.
- Wang, S., Fang, X., Zheng, D. and Wang, E., 2009, Initiation of slip along the Xianshuihe fault zone, eastern Tibet, constrained by K/Ar and fission-track ages: *International Geology Review*, v. 51, p. 1121-1131, doi:10.1080/00206810902945132

- Wang, Q., Zhang, P.Z., Freymueller, J.T. and 10 others, 2001, Present-day crustal deformation in China constrained by global positioning system measurements: *Science*, v. 294, p. 574-577.
- Wang, Q., Chung, S.-L., Li, X.-H. and 7 others., 2015, Mid-Miocene to Quaternary crustal melting beneath northern Tibet. *Earth and Planetary Science Letters*, in review.
- Wei, W., Unsworth, M., Jones, A. and 12 others, 2001, Detection of widespread fluids in the Tibetan crust by magnetotelluric studies: *Science*, v. 292, p. 716-718.
- Weller, O.M., St-Onge, M.R., Waters, D.J., Rayner, N., Searle, M.P., Chung, S.-L., Palin, R.M., Lee, Y.-H. and Xu, X., 2013, Quantifying Barrovian metamorphism in the Danba structural culmination of eastern Tibet: *Journal of Metamorphic Geology*, v. 31, p. 909-935, doi:10.1111/jmg.12050
- Weller, O.M., St-Onge, M.R., Searle, M.P., Waters, D.J., Rayner, N., Chen, S., Chung, S.-L., and Palin, R.M., 2015, Quantifying the P-T-t conditions of north-south Lhasa terrane accretion: new insight into the pre-Himalayan architecture of the Tibetan plateau: *Journal of Metamorphic Geology*, v. 33, p. 91-113, doi:10.1111/jmg.12112
- Weller, O.M., St-Onge, M.R., Searle, M.P., Waters, D.J. and Rayner, N., 2016, Miocene magmatism in the Western Nyainqentanglha mountains of southern Tibet: An exhumed bright spot?, *Lithos*, v. 245, p. 147-160, doi:10.1016/j.lithos.2015.06.024
- Wen, D.-R., Liu D., Chung, S.-L. and 7 others, 2008a, Zircon SHRIMP U-Pb ages of the Gangdese Batholith and implications for Neotethyan subduction in southern Tibet: *Chemical Geology*, v. 252, p. 191-201.
- Wiedenbeck, M. A. P. C., Alle, P., Corfu, F., Griffin, W. L., Meier, M., Oberli, F., Von Quadt, A., Roddick, J. C., & Spiegel, W., 1995. Three natural zircon standards for U-Th-Pb, Lu-Hf, trace element and REE analyses. *Geostandards newsletter*, v. 19(1), p. 1-23.
- Wilson, C.J.L., Harrowfield, M.J. and Reid, A.J., 2006, Brittle modification of Triassic architecture in eastern Tibet: implications for the construction of the Cenozoic plateau: *Journal of Southeast Asian Earth Sciences*, v. 27, p. 341-357.
- Xu, X., Wen, X., Zheng, R., Ma, W., Song, F. and Yu, G., 2003, Pattern of latest tectonic motion and its dynamics for active blocks in Sichuan-Yunnan region, China: *Science in China*, v. 46, p. 210-226, doi:10.1360/03dz0017.
- Zhang, P., Molnar, P., Burchfiel, B. C., Royden, L., Wang, Y., Deng, Q., Song, F., Zhang, W. and Jiao, D., 1988, Bounds on the Holocene Slip Rate of the Haiyuan Fault, North-Central China: *Quaternary Research*, v. 30, p. 151-164.
- Zhang, P., Molnar, P. and Xu, X., 2007, Late Quaternary and present-day rates of slip along the Altyn Tagh Fault, northern margin of the Tibetan Plateau, *Tectonics*, v. 26, doi: [10.1029/2006TC002014](https://doi.org/10.1029/2006TC002014)
- Zhang P.Z., Shen, Z., Wang, M., GAN, W.J., Molnar, P., Burgman, R. and Molnar, P., 2004, Continuous deformation of the Tibetan Plateau from global positioning system data: *Geology*, v. 32, p. 809-812.

Zhang, H., Harris, N., Guo, L. and Xu, W., 2009, The significance of Cenozoic magmatism from the western margin of the eastern syntaxis, southeast Tibet: Contributions to Mineralogy and Petrology, doi: 10.1007/s00410-009-0467-5

Zhang, Z.M., Zhao, G.C., Santosh, M., Wang, J.L., Dong, X. and Liou, J.G., 2010, Two stages of granulite facies metamorphism in the eastern Himalayan syntaxis, south Tibet: petrology, zircon geochronology and implications for the subduction of Neo-Tethys and the Indian continent beneath Asia: Journal of Metamorphic Geology, v. 28, p. 719-733.

Zhang, Z, Yuan, X., Chen, Y., Tian, X., Kind, R., Li, X., and Teng, J., 2010, Seismic signature of the collision between the eastern Tibet escape flow and the Sichuan basin: Earth and Planetary Science Letters, v. 292, p. 254-264.

Zhang, H., Zhao, D., Zhao, J. and Xu, Q., 2012, Convergence of the Indian and Eurasian plates under eastern Tibet revealed by seismic tomography: Geochemistry, Geophysics, Geosystems, v. 13, doi: 10.1029/2012GC004031

Zhou, M-F., Yan, D-P., Kennedy, A.K., Li, Y. and Ding, J., 2002, SHRIMP U-Pb zircon geochronological and geochemical evidence for Neoproterozoic arc-magmatism along the western margin of the Yangtze Block, South China: Earth and Planetary Science Letters, v. 196, p. 51-67.

## FIGURE CAPTIONS

**Fig. 1.** Digital Elevation Map of the Tibetan plateau showing the main active faults, sutures and terranes (after Taylor and Yin, 2009). The location of Gongga Shan peak (7556 m) is shown by the red triangle.

**Fig. 2.** Fault map of the Eastern Tibetan Plateau showing the major strike-slip faults (after Taylor and Yin, 2009) including the left-lateral Xianshuihe fault and the location of the Gongga Shan granite batholith.

**Fig. 3. (a)** Landsat-7 mosaic satellite image of eastern Tibet with major faults overlaid. **(b)** Enlarged Landsat-7 satellite image of Gongga Shan batholith. The three main transects studied in this paper, Kangding road section, Yanzigou valley north of Gongga Shan, and the Hailuoguo valley west of Moxi, leading up to Gongga Shan peak (7556 m) are shown.

**Fig. 4.** Map of the Gongga Shan batholith and adjacent parts of eastern Tibet (after Sichuan Bureau of Geology and Mineral Resources (1981) and Harrowfield et al. (2005), showing locations of all samples dated in this paper together with those of Roger et al. (1995) and Li and Zhang (2013).

**Fig. 5.** Field outcrop photos, Kangding section: (a) Sample BO-59 biotite granite with enclave of earlier granodiorite, from the western margin of the Gongga Shan batholith above Kangding new airport. (b) Sample BO-62, a biotite + K-feldspar monzogranite typical of much of the batholith. (c) Shuguang bridge locality, Kangding road. Biotite monzogranite (BO-57) has been intruded by a second phase more leucocratic biotite ± muscovite granite (BO-52) with migmatitic textures (schlieren of melanosome). Both lithologies are cut by a later undeformed pegmatite (BO-55). (d) Late garnet leucogranite (e) Complex intrusive phase of later leucogranite (pale) intruding earlier biotite granite. (f) Biotite microgranite sill, the youngest phase of magmatism in the Kangding profile.

**Fig. 6. (a)** Western margin of the Gongga Shan batholith at Zheduo Shan pass, Kangding road, vertical intrusive contact into Triassic black shales. **(b)** four phases of granite intrusions from early biotite monzogranite through to late garnet + biotite leucogranite cut by pegmatite dykes immediately west of Kangding town. **(c)** biotite + hornblende granodiorites with igneous enclaves, Conch gully area south of Kangding. **(d)** magmatic mixtures of more enclave-rich granite intermingled with the granodiorite. **(e)** and **(f)** garnet leucogranite with minor muscovite and lacking in biotite and hornblende, Conch gully.

**Fig. 7.** Field outcrop photos from Yanzigou valley north of Gongga Shan. (a) East-verging recumbent folds in probable Triassic meta-sediments. (b) Yanzigou spires composed of foliated biotite + hornblende granodiorites (BO-76). (c) Swallow cliffs area and around the snout of the north Gongga Shan glacier showing five phases of cross-cutting granites. (d) leucogranites (BO-62) intruding into and breaking up enclaves of the more mafic granites. (e) Multiple phases of cross-cutting granitoids from the middle part of the batholith. (f) Foliation in granodiorites striking  $160^{\circ}$  NW-SE and dipping at  $50^{\circ}$  NE at eastern margin of the batholith.

**Fig. 8.** At least seven phases of cross-cutting granites in one outcrop along the Yanzigou valley, in general with earlier diorite-granodiorite phases cut by increasing more leucocratic granites.

**Fig. 9.** Field outcrop photos from Hailuogou valley. (a) Peak of Gongga Shan (7556 m) composed mainly of granodiorite at the western margin of the batholith. (b) Vertical eastern margin of the Gongga Shan batholith above Hailuogou valley showing granite contact cutting west-dipping foliation in the meta-sediments. (c) hornblende + biotite diorite with K-feldspar megacrystic granite also containing hornblende and biotite above cable car station Hailuogou glacier. (d) Igneous diorite enclaves within the Gongga Shan granite.

**Fig. 10.** Concordia (zircon) and Tera-Wasserburg (allanite) plots for sample BO52, and representative CL images of zircons with analyses shown. Grey ellipses (zircon) are excluded from the tuffzirc age calculation shown, and are inherited or relate to younger zircon growth/lead-loss. Grey ellipses (allanite) are excluded from intercept age calculations and are presumably age mixtures.

**Fig. 11.** Concordia (zircon) and Tera-Wasserburg (allanite) plots for sample BO55, and representative CL images of zircons with analyses shown. Grey ellipses (allanite) are mixing between an older (defined by the black ellipses) and younger component.

**Fig. 12.** Concordia (zircon) plots for samples BO57 and BO59, and Tera-Wasserburg (allanite) plot for sample BO59 with representative CL images of zircons with analyses shown. Grey ellipses (zircon) are excluded from age calculations, and are inherited or feature lead-loss. Grey ellipses (allanite) are mixing between an older (defined by the black ellipses) and younger component.

**Fig. 13.** Concordia (zircon) and Tera-Wasserburg (allanite) plots for samples BO62 and BO59, and representative CL images of zircons with analyses shown. Grey ellipses are analyses that comprise a significant common-lead component, blue

ellipses are those that are mixing between ca. 15 Ma and ca. 800 Ma components, and black ellipses are analyses that are mixing between ca. 5 and ca. 800 Ma.

**Fig. 14.** Concordia (zircon) and Tera-Wasserburg (allanite) plots for samples BO68, and representative CL images of zircons with analyses shown. Grey ellipses (zircon) are excluded from age calculations, and are inherited or feature lead-loss.

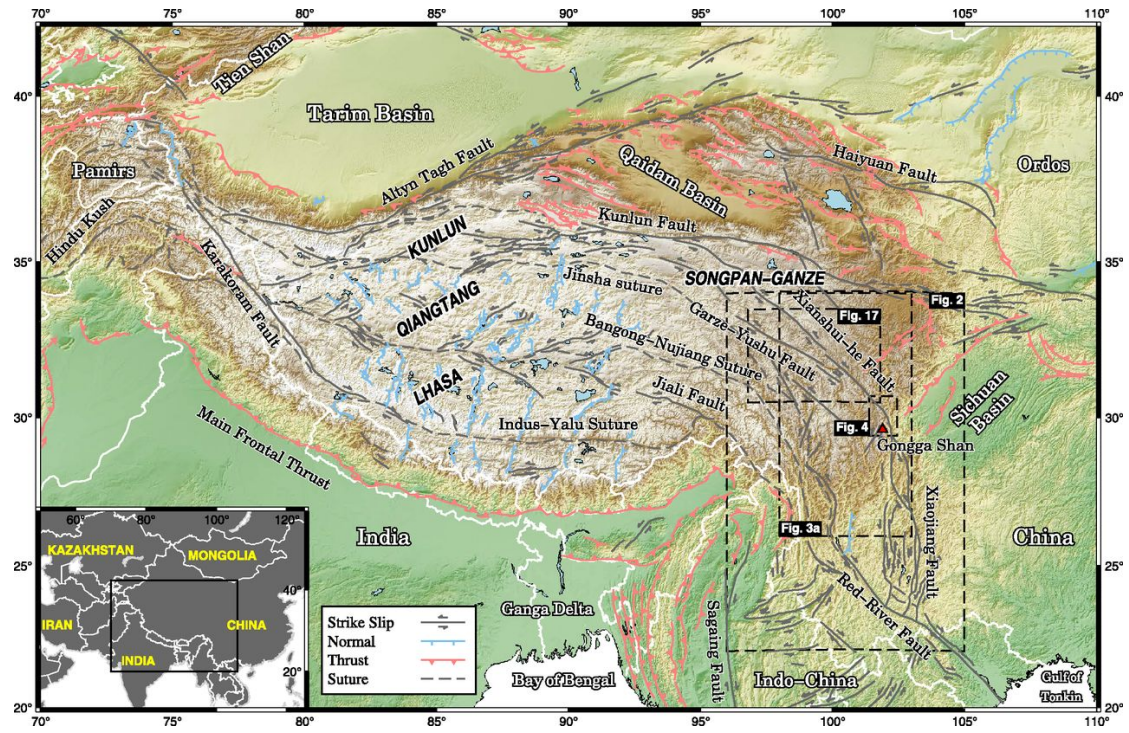
**Fig. 15.** Concordia (zircon) and Tera-Wasserburg (allanite and titanite) plots for samples BO76, and representative CL images of zircons with analyses shown. Grey ellipse (zircon) comprises a common lead component. Grey ellipses (titanite) are excluded from age calculation, and are disturbed due to a younger event or minor open-system behaviour.

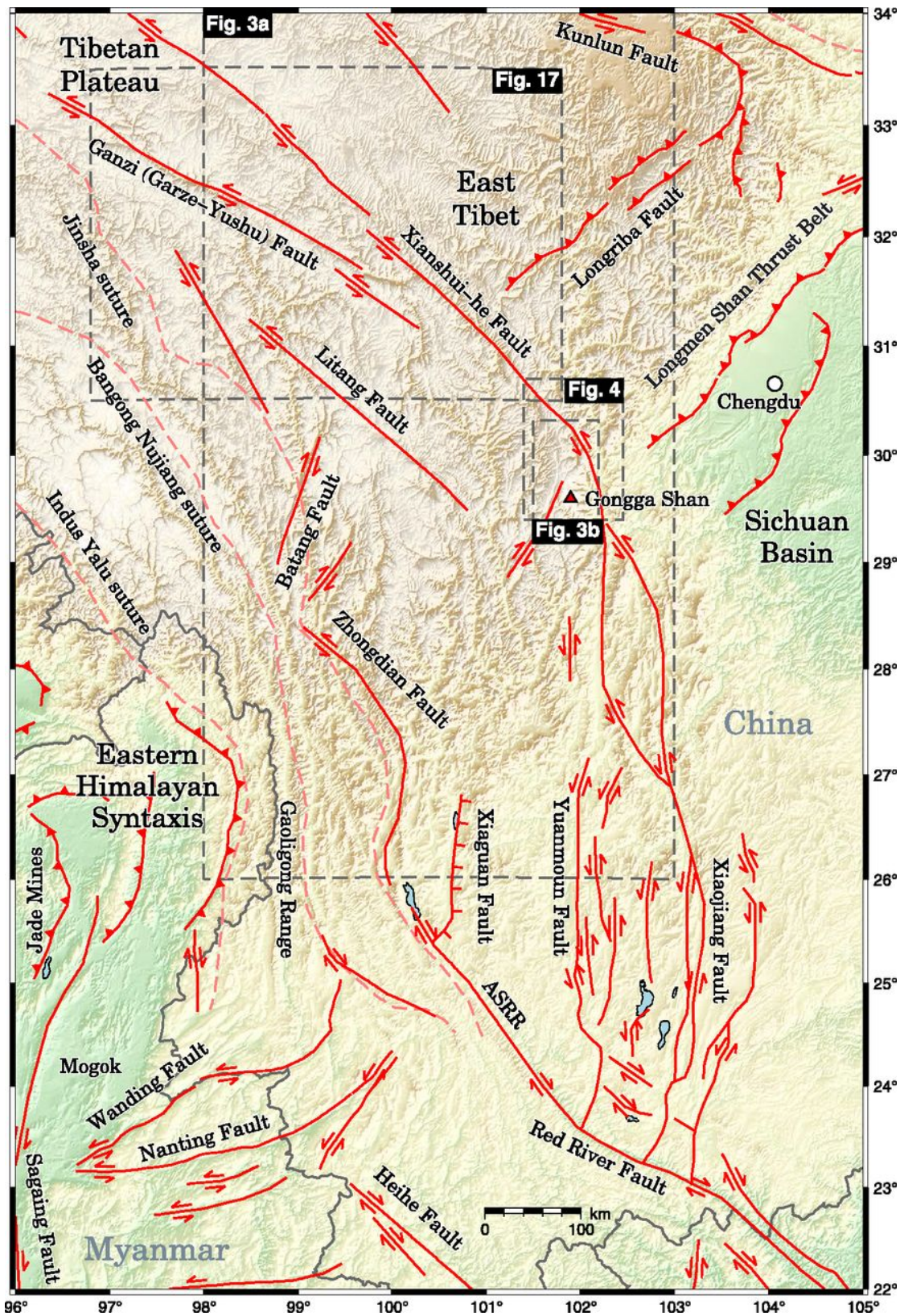
**Fig. 16.** Compilation of U-Pb zircon, titanite, allanite data from this study, compared to previous studies. Grey bands are tectonothermal events based on geochronologic data of this study, all of which include granite melting.

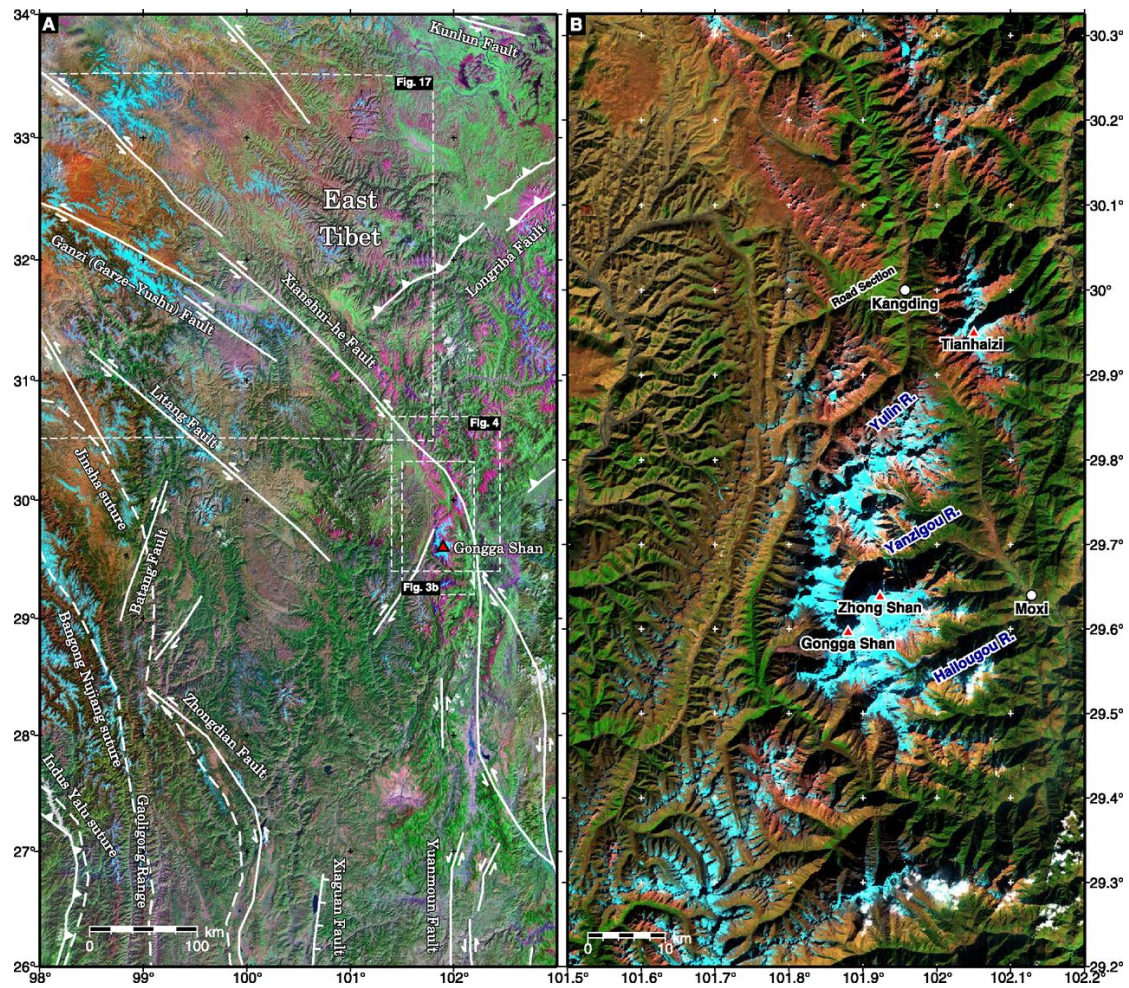
**Fig. 17.** Landsat map of the Gerze-Yushu fault and Xianshui-he fault showing offset river courses of the Jinsha and upper Yangtze rivers. Offsets estimated from pinning points of valleys could vary by up to 5km.

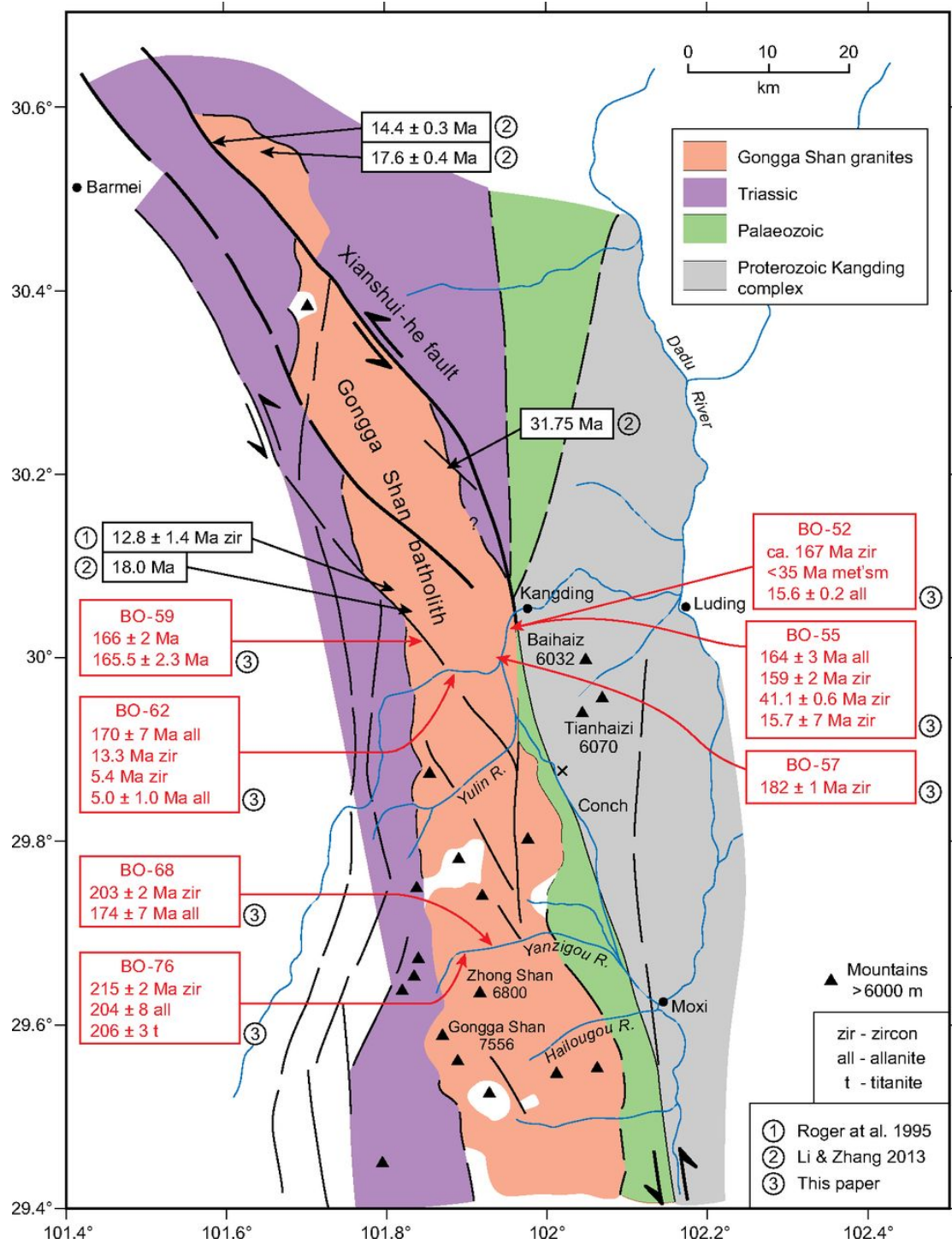
## **SUPPLEMENTARY FILE**

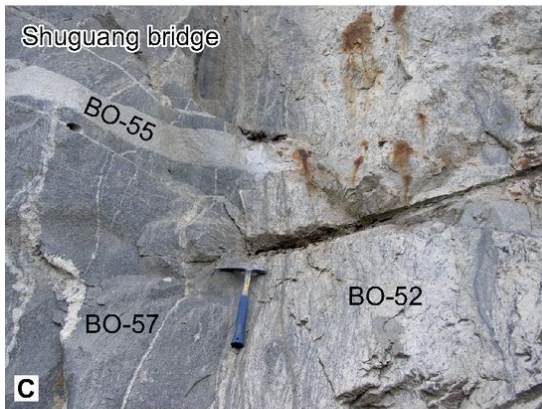
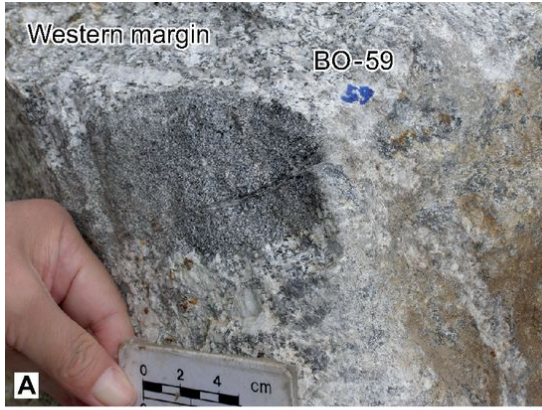
Analytical Conditions



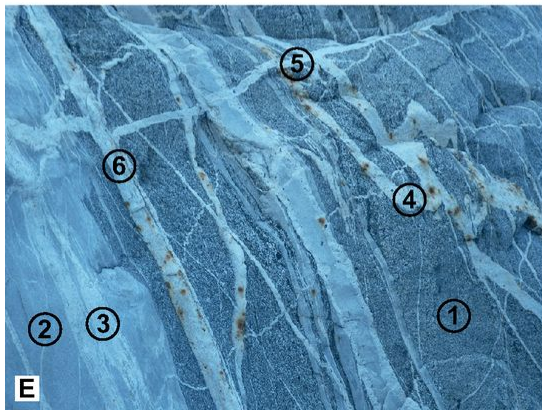
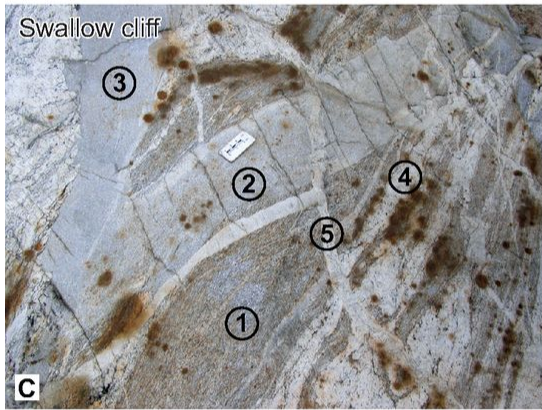
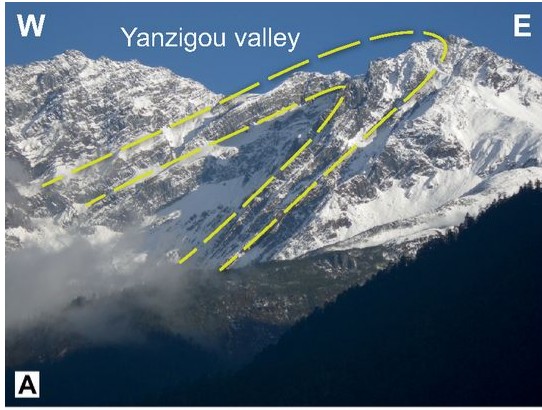


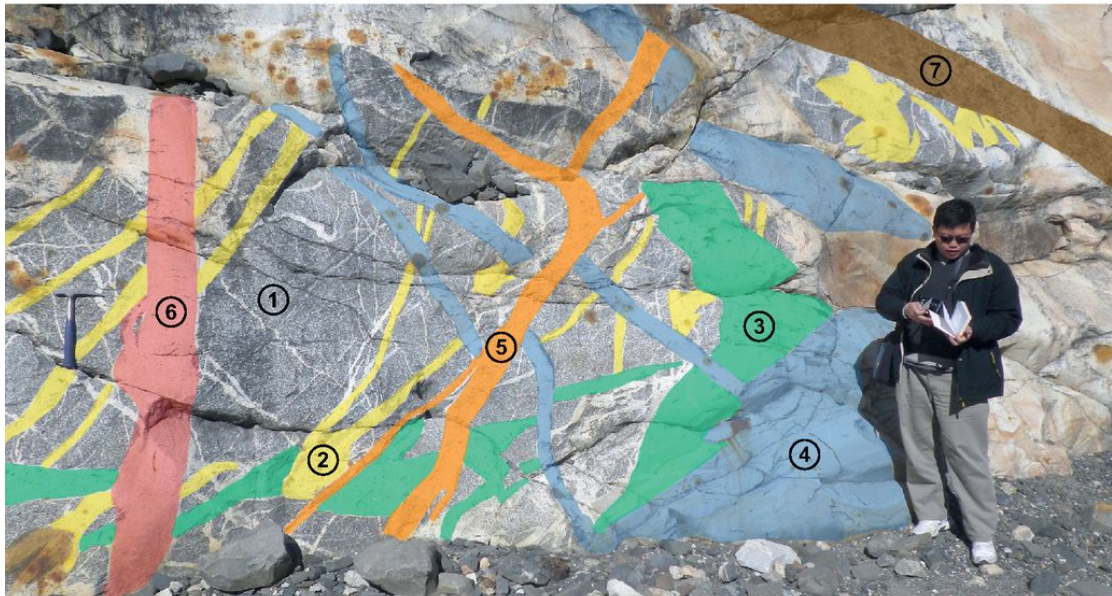












- |   |  |
|---|--|
| <ul style="list-style-type: none"> <li><span style="border: 1px solid black; padding: 2px;">4</span> Fine-grained Bt leucogranite</li> <li><span style="border: 1px solid black; padding: 2px;">3</span> Darker Bt granite</li> <li><span style="border: 1px solid black; padding: 2px;">2</span> Bt leucogranite</li> <li><span style="border: 1px solid black; padding: 2px;">1</span> Bt + Hbl granodiorite</li> </ul> <p>oldest</p> | <p>youngest</p> <ul style="list-style-type: none"> <li><span style="border: 1px solid black; padding: 2px;">7</span> Coarse-grained Kfs + Bt ± Ms pegmatite</li> <li><span style="border: 1px solid black; padding: 2px;">6</span> Grt + Bt leucogranite</li> <li><span style="border: 1px solid black; padding: 2px;">5</span> Coarse-grained Bt granite</li> </ul> |
|---|--|

